FACULTY OF SCIENCE AND TECHNOLOGY

BACHELOR'S THESIS

Study programme / specialisation: Civil engineering / Structural engineering	The spring semester, 2023 Open / ~~Confidential~~
Author: Marie Heng Bjoland	
Supervisor at UiS: Fredrik Bjørheim External supervisor(s): Jonas R. Kildal	
Thesis title: Comparison of Joint Geometry of an Offshore Fish Farm	
Credits (ECTS): 20	
Keywords: FEM Sesam GeniE Joint geometry Fish Farm	Pages: 96 + appendix: 0 Stavanger, *15.05.2023*

ABSTRACT

This thesis was written in collaboration with Global Maritime (GM), and its aim is to compare two geometrically different structural joints on an offshore fish farm, named GM Aqua Design. The two models are compared on four main criteria: the structural integrity, the functionality, the constructability, and the material usage. The two models, a conic-model and a box-model are prepared and analysed in Sesam GeniE. The results from the analysis show that the two models both fulfil the structural integrity requirements with respect to stress level and displacements. The conic-model has a range of issues related to functionality and constructability due to the curved plates, that dominates over the fact that the box-model requires 10% more material. After an overall evaluation the box-model is recommended.

ACKNOWLEDGEMENT

I would like to thank Global Maritime for their hospitality and giving me the opportunity to write this thesis. I will also thank them for letting me work on this thesis at their office, where I was allowed to use their computer and GeniE license.

Special thanks to Jonas Kildal, Line Kristiansen and Arne Vagle at Global Maritime for their support and valuable discussion.

I would also like to thank my supervisor Fredrik Bjørhem at UiS for his support.

TABLE OF CONTENT

LIST OF FIGURES

LIST OF TABLES

LIST OF EQUATIONS

1 INTRODUCTION

The Norwegian aquaculture industry had its breakthrough in the 1970's when the first harvest of salmon from sea water succeeded [1]. Since then, the industry has been in continuous development and growth. Today aquaculture has become a major industry along the coast of Norway because of increased knowledge and improved technologies. As a result of this aquaculture is today Norway's second largest export industry [2].

The Norwegian government considers "Combing the preservation of clean and healthy oceans with sustainable use." [2] as one of its most important tasks. Since Norway is the world's largest exporter and farmer of Atlantic salmon and rainbow trout, the nation has a key role in the production of sustainable food globally. The Norwegian government's priority is not unique, the United Nation also aim to "Conserve and sustainably use the oceans, seas and marine resources for sustainable development" [3]. In fact, this statement is one of the 17 Sustainable Development Goals (SDGs) adopted by United Nation Member States in 2015. The SDGs are a "universal call to action to end poverty, protect the planet and improve the live and prospects of everyone, everywhere". [3]

1.1 Offshore Fish Farms

The Norwegian costal line with its many islands and fjords has been proved to be excellent for traditional fish farming, as it provides shelter. However, further expansion of the aquaculture industry in a traditional manner is no longer recognized as sustainable by the Norwegian Ministry of Trade, Industry and Fisheries due to acreage and environmental challenges. Therefore, the ministry of Trade, Industry and Fisheries encourages companies to look at more exposed areas.

Ocean Farm 1 (OF1) was the world's first offshore fish farm, located at Frohavet and was awarded the first development license by the Ministry of Trade, Industry and Fisheries. The Ministry developed these licenses to motivate companies to invent solutions to the challenges the aquaculture industry is facing.

1.1.1 GM Aqua Design

GM Aqua Design is a modular solution. The design is developed by Moreld Aqua and as of today designed for semi exposed locations with significant wave hight, $H_{s,}$ of less than 8 meters. There is also a project working towards fully exposed locations (areas with even higher significant wave hights). More exposed areas would make new areas available, and thus increase the aquaculture industry, while being more sustainable than traditional fish farming.

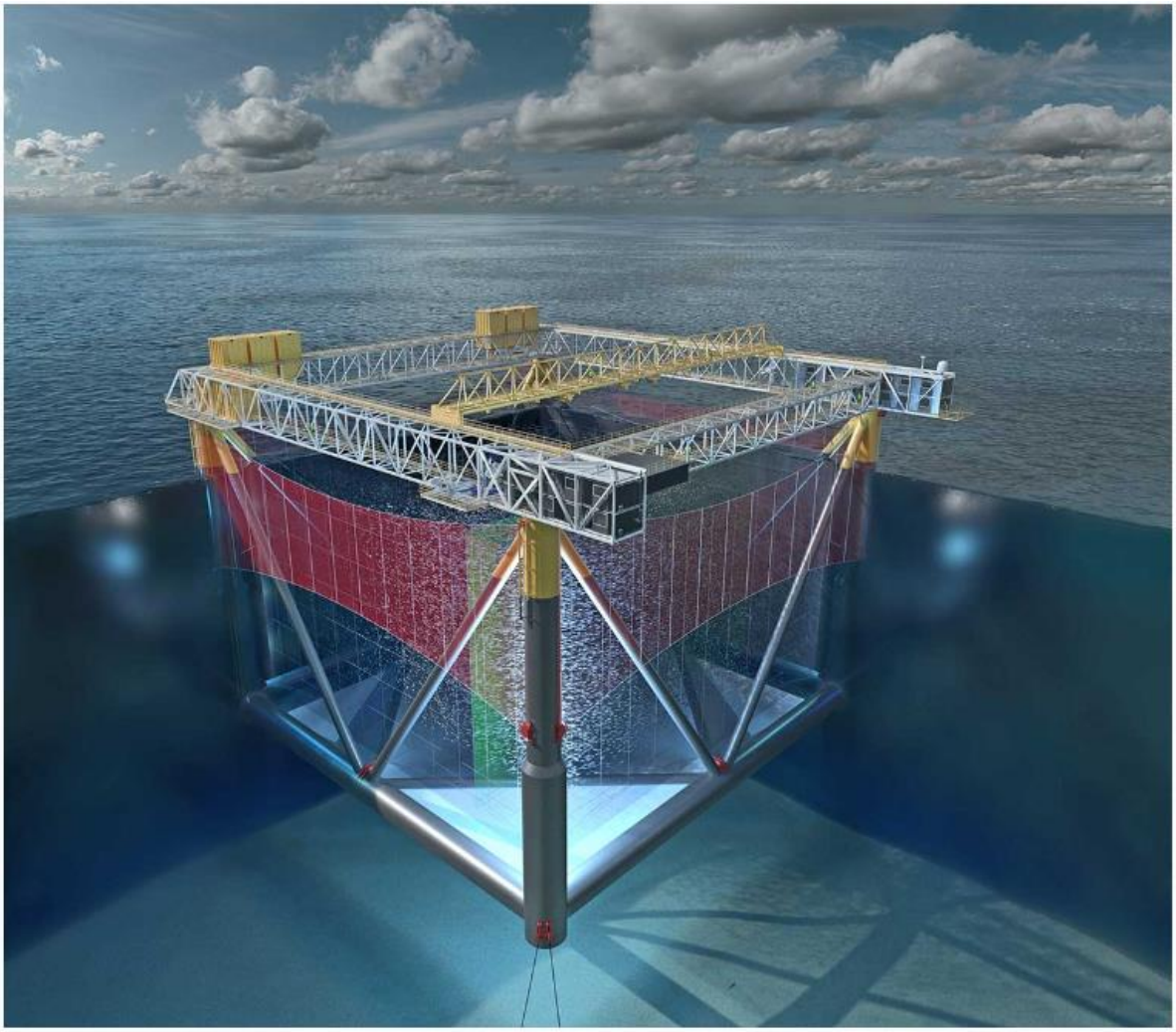

Figure 1-1 GM Aqua Design (illustration supplied by GM)

1.2 Objective

The objective of this thesis is to compare two local models of geometrically different joints on an offshore fish farm, GM Aqua Design. The joints will be modelled in Sesam GeniE as shells with internal structure consisting of stiffeners modelled as beams. The models will be compared by performing a linear static analysis at the Ultimate Limit State (ULS). Loads from the ULS load case are applied as displacement on the boundary cut sections and are a result of analysis of the load case on a global model of the fish farm performed by Global Maritime.

The models are compared based in the following four criteria:

a) Structural integrity – the joints ability to sufficiently withstand the applied loads. In this thesis the structural integrity of the two models is compared based on results from displacements and von Mises stress.
b) Functionality – the accessibility to equipment such as pumps.
c) Constructability – the accessibility to perform necessary welding and surface finishing such as sand blasting and painting as well as the fabrication complexity.
d) Material usage – the material usage is closely related to the cost of the joint.

The models and their differences are described in detail in section 6.3, 6.4 and 6.5. Sesam GeniE is presented in chapter 5

1.3 Limitations

Several limitations are set to limit the extension of this thesis:

- Only Ultimate Limit State (ULS) for one load case is considered.
- Only a linear static analysis is performed.
- Buckling is not evaluated.
- Accidental limit state (ALS) is not considered.
- Serviceability Limit Sate (SLS) is not considered for operation.
- Fatigue Limit State (FLS) is not considered in detail
- Deformation loads are not considered.
- Material selection is not under scope by this thesis.
- Hydrodynamic loads from motion response analysis are not considered.
- Lamellar tearing is not considered.
- True thickness stress nor material properties are not evaluated

1.4 Outline

The outline of the main chapters of this thesis are:

Chapter 1: Introduction

Chapter 2, 3 and 4: The main theory used in this thesis is presented

Chapter 5: Presents Sesam software and Sesam GeniE

Chapter 6: The modelling of the joints

Chapter 7: The analysis performed

Chapter 8: The results for Xtract are presented

Chapter 9: Discussion of the results

Chapter 10: Recommendations of future work

Chapter 11: Summary and conclusion

2 STATIC ANALYSIS

2.1 Limit State Design

Limit state is defined by Det Norske Veritas (DNV) as “a condition beyond which a structure or a part of a structure exceeds a specified design requirement” [4]. Several limit states are considered during a structural analysis, the four most common are described by DNV as [4]:

- Ultimate Limit State (ULS) – ultimate resistance for carrying load
- Serviceability Limit State (SLS) – criteria applicable to normal use or durability
- Fatigue Limit State (FLS) – related to possibility of failure due to cyclic loads
- Accidental Limit State (ALS)- damage due to accidental event or operational failure [4]

Examples of Ultimate Limit States described by DNV [4]:

- Loss of structural resistance (excessive yielding and buckling)
- Failure of components due to brittle fracture
- Loss of static equilibrium of the structure, or of a part of the structure
- Failure of critical components of the structure caused by exceeding the ultimate resistance or deformation of the components
- Transformation of the structure into a mechanism (collapse or excessive deformation). [4]

2.2 Linear Static Analysis

Even though there are several different types of structural analysis, the most common is linear static. Other analysis types include nonlinear and dynamic. Linear static analysis is the most used due to simplicity, speed, and availability (The basic package of most software is linear static) [5].

2.2.1 Linear Assumption

Three main assumptions must be valid for a linear analysis to be suitable [5].

- Material properties
- Geometric concerns
- Boundary conditions

A material is considered linear if the relationship between stress and strain is assumed to be linear, it must comply with Hook's Law. The stress, σ, is linearly proportional to its strain, ε, by the modulus of elasticity, E [5].

$$\sigma = E \cdot \varepsilon$$ *Eq. 2-1 Hook's Law*

The biggest geometric concern for the linear assumption is geometric stiffening, also known as stress stiffening. Geometric stiffening is stiffening over and beyond the material properties and is primarily a result of increased tensile stresses in areas being deformed. As the axial tensile stress in a beam or the in-plane tension in a shell increases the element will self-stiffen. Geometric stiffening is primarily a concern in structures with bending stiffness very small compared to the axial stiffness. The primary result of geometric stiffening is proportionally decreasing displacement under increasing load [5].

The effect of geometric stiffening is accounted for in finite element analysis by adding an additional stiffness matrix, often referred to as the stress stiffness matrix. The stress stiffness matrix is added to the stiffness matrix to give the total stiffness matrix [6].

The boundary conditions are considered linear if they do not change from the point of load application to the final deformed shape. In addition, the loading must be constant in magnitude, orientation, and distribution for the linear assumption to be valid [5].

2.2.2 Static Assumption

For the static assumption to be valid the load applied must be considered as a static load. Static loads are loads that are applied gradually to their full magnitude, and do not change over time [5].

2.3 Von Mises Stress

Failure is usually considered to occur at the onset of plastic deformation for a ductile material and at fracture for brittle materials. These points are easy to define for a tensile test, such as a uniaxial test. However, for tri-axial cases predicting failure is difficult, and one universally applicable test method does not exist. Instead, the most suitable failure theory must be chosen from a range of failure theories. Some examples of failure theories are Rankine, Tresca and von Mises. Based on certain circumstances and results from experiments it is possible to find a failure theory that works relatively well [7].

For a failure theory to be suitable, it must be consistent with the observations made from previous failure experiments. For ductile materials one of the key observations needed to be covered is related to hydrostatic stresses as they do not cause yielding in ductile materials. This is because yielding of a ductile material is caused by shear deformation and since there are no shear forces (and thus no shear stress) caused by hydrostatic stresses, no yielding can occur [7].

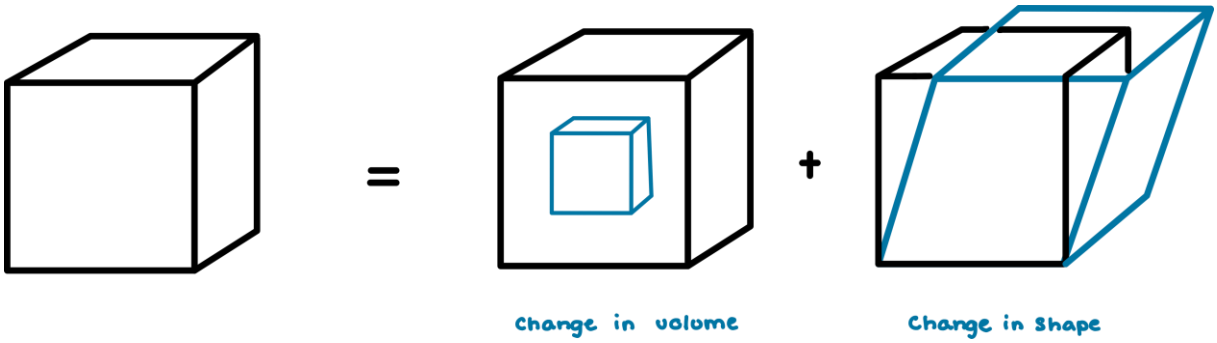

Figure 2-1 Triaxial Stress

A tri-axial stress situation can de decomposed into stresses causing distortion of shape and stresses causing change in volume. Hydrostatic stresses cause a change in volume of the object. For a hydrostatic stress, the three principal stresses are always equal [7].

$$\sigma_1 = \sigma_2 = \sigma_3$$

Eq. 2-2 Hydrostatic stress Principal Stresses

As a result, the hydrostatic pressure can be calculated as the average of the three principal stresses [7]:

$$\sigma_{avg} = \frac{\sigma_1 + \sigma_2 + \sigma_3}{3}$$

Eq. 2-3 Average Hydrostatic Stress

The stress causing a distortion of shape is called deviatoric stress. This can be found for each principal stress, by subtracting the hydrostatic stress from the principal stress component. The deviatoric stresses are responsible for yielding because they cause shear stress and changes in shape. Thus, deviatoric stresses causes failure in ductile materials [7].

$$\sigma_{d1} = \sigma_1 - \sigma_{avg}$$

Eq. 2-4 Deviatoric stress, σ_{d1}

$$\sigma_{d2} = \sigma_2 - \sigma_{avg}$$

Eq. 2-5 Deviatoric stress σ_{d2}

$$\sigma_{d3} = \sigma_3 - \sigma_{avg}$$

Eq. 2-6 Deviatoric stress σ_{d3}

The forces can be expressed as matrices [7]:

$$\sigma = \begin{bmatrix} \sigma_1 & 0 & 0 \\ 0 & \sigma_2 & 0 \\ 0 & 0 & \sigma_3 \end{bmatrix} = \begin{bmatrix} \sigma_{avg} & 0 & 0 \\ 0 & \sigma_{avg} & 0 \\ 0 & 0 & \sigma_{avg} \end{bmatrix} + \begin{bmatrix} \sigma_1 - \sigma_{avg} & 0 & 0 \\ 0 & \sigma_2 - \sigma_{avg} & 0 \\ 0 & 0 & \sigma_3 - \sigma_{avg} \end{bmatrix}$$

Eq. 2-7 Forces

This can be further developed for any arbitrary orientation, and thus include shear stresses , τ_{xy}, τ_{zx} and τ_{yz} [7]:

$$\sigma = \begin{bmatrix} \sigma_1 & \tau_{xy} & \tau_{zx} \\ \tau_{xy} & \sigma_2 & \tau_{yz} \\ \tau_{zx} & \tau_{yz} & \sigma_3 \end{bmatrix} = \begin{bmatrix} \sigma_{avg} & 0 & 0 \\ 0 & \sigma_{avg} & 0 \\ 0 & 0 & \sigma_{avg} \end{bmatrix} + \begin{bmatrix} \sigma_1 - \sigma_{avg} & \tau_{xy} & \tau_{zx} \\ \tau_{xy} & \sigma_2 - \sigma_{avg} & \tau_{yz} \\ \tau_{zx} & \tau_{yz} & \sigma_3 - \sigma_{avg} \end{bmatrix}$$

Eq. 2-8 Forces in Any Arbitary Orientation

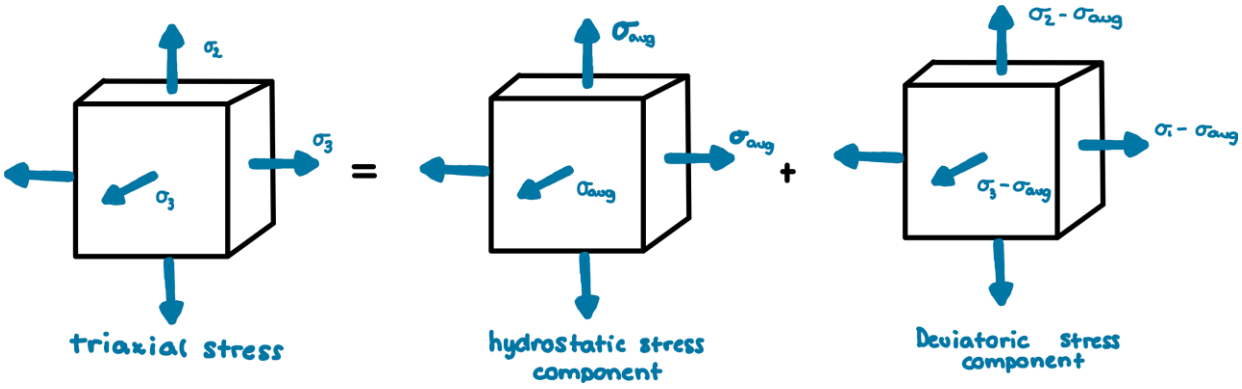

Figure 2-2 Hydrostatic and Deviatoric Stress

The von Mises failure criteria also known as the maximum distortion energy theory is one of the most common failure theories for ductile materials, such as steel. It states:

"Yielding occurs when the maximum distortion energy, u_d, is equal to the distortion energy at yielding in a uniaxial tensile test, $u_{d,y}$" [7]

$$u_d = u_{d,y}$$

Eq. 2-9 Von Mises Criteria

The distortion energy is the portion of strain energy corresponding to the effect of the deviatoric stresses. The distortion energy per unit volume can be calculated from the equation [7]:

$$u_d = \frac{1+\nu}{6E}[(\sigma_1 - \sigma_2)^2 + (\sigma_2 - \sigma_3)^2 + (\sigma_3 - \sigma_1)^2]$$

Eq. 2-10 Distortion Energy

The principal stresses at yielding are [7]:

$$\sigma_1 = \sigma_y$$ *Eq. 2-11 Principal Stress at Yielding, σ_1*

$$\sigma_2 = 0$$ *Eq. 2-12 Principal Stress at Yielding, σ_2*

$$\sigma_2 = 0$$ *Eq. 2-13 Principal Stress at Yielding, σ_3*

Where σ_y is the yielding stress for the material:

$$u_{d,y} = \frac{1+\nu}{6E}\left[\left(\sigma_y - 0\right)^2 + (0-0)^2 + \left(0-\sigma_y\right)^2\right] = \frac{1+\nu}{6E}{\sigma_y}^2$$ *Eq. 2-14 Distortion enegy*

Rearranging the equation:

$$\sqrt{\frac{1}{2}[(\sigma_1-\sigma_2)^2 + (\sigma_2-\sigma_3)^2 + (\sigma_3-\sigma_1)^2]} = \sigma_y$$ *Eq. 2-15 Von Mises stress*

For any arbitrary orientation

$$\sqrt{\frac{1}{2}[(\sigma_1-\sigma_2)^2 + (\sigma_2-\sigma_3)^2 + (\sigma_3-\sigma_1)^2] + 3\left({\tau_{xy}}^2 + {\tau_{yz}}^2 + {\tau_{xz}}^2\right)} = \sigma_y$$ *Eq. 2-16 Arbitrary Von Mises*

The term on the left is called the equivalent von Mises stress. If the equivalent von Mises stress is greater than the yield strength, yielding is predicted to have occurred. The equivalent von Mises stress is a common output in stress analysis from finite element method (FEM) to allow areas in risk of yielding to be identified [7].

The representation of a failure theory in the principal stress space is called a yield surface. The yield surface for von Mises stress is an ellipse for plane stress

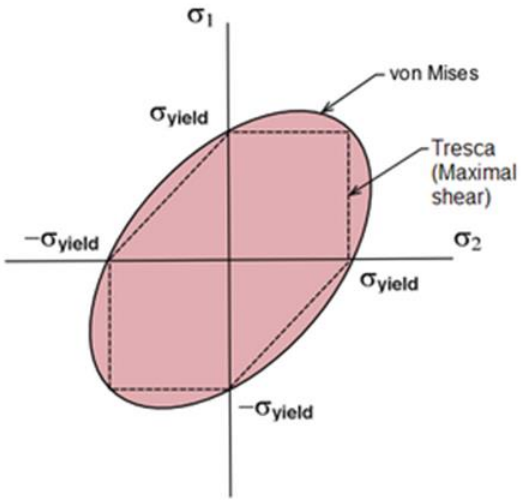

Figure 2-3 Yield surafce von Mises, [21]

2.3.1 Von Mises of the membrane

Membrane stresses occur in plate and shell elements. Membrane stresses are extracted in the mid-plane of the plate/shell. In most cases the mid-plane correlates with the neutral-bending-plane. Thus, the effect of bending stresses are neglected in most cases in the membrane results [7].

2.4 Curved Shells

2.4.1 Hoop Stress

The stresses acting in the walls of a cylindrical or spherical pressure vessels can be analysed in a simple manner, provided that the vessels have thin walls. The walls are recognised as thin if the inner-radius-to-wall thickness ratio is 10 or more [8].

$$\frac{r}{t} \geq 10$$

Eq. 2-17 Thin wall criteria

For an r/t- ratio of 10 the calculated maximum stress is approximately 4% less than the actual maximum stresses For larger r/t-ratios this error will be less [8].

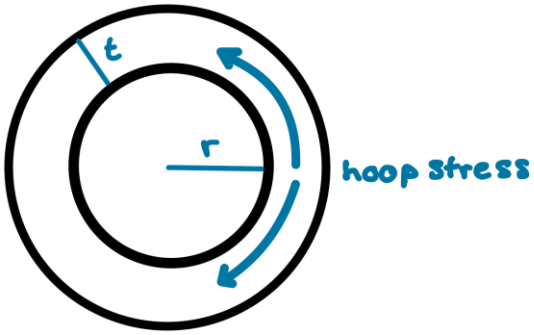

Figure 2-4 Hoop stress

The circumferential or hoop stress, σ_θ , can be determined from:

$$\sigma_\theta = \frac{P \cdot r}{t}$$

Eq. 2-18 Hoop stress

Where P is the pressure acting on the vessel, r the inner radius and t the thickness of the shell

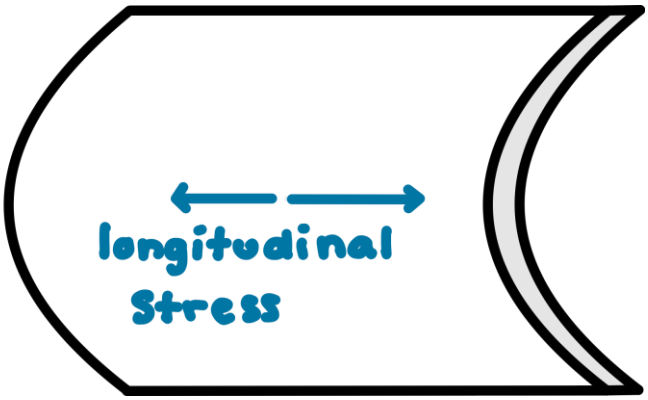

Figure 2-5 Longitudinal stress, cylinder

The longitudinal or axial stress in a cylinder can be calculated from the same parameters [8]:

$$\sigma_a = \frac{P \cdot r}{2 \cdot t}$$

Eq. 2-19 Axial stress, cylindrical shell

2.4.2 Benefits of curvature

The curvature of a curved shell will cause reduced bending stresses in the section when compared with an equivalent section consisting of flat plates such as rectangular hollow sections. This reduction is a result of stresses that are transferred as bending stresses in a flat section being transferred as membrane stresses in the curved shells, hoops stresses [7].

2.5 Static Loads

2.5.1 Hydrostatic Pressure

An object submerged in a fluid (liquid or gas) will be subject to a fluid pressure distributed over its surface, for liquids this is called hydrostatic pressure. The only pressure dealt with in fluid statics is the normal stress, and its variation is only due to the weight of the fluid. There is no shear stress in fluid statics as there are no relative motion between adjacent fluid layers. In addition, the are no shear forces between the fluid and the object as there are no relative motion between them [9]. It is common to work with the gage pressure when dealing with hydrostatic pressure problems. The hydrostatic gage pressure, P_{gage}, for an incompressible liquid, i.e., water, is calculated as [9]:

$$P_{gage} = \rho g h$$ *Eq. 2-20 Hydrostatic Pressure*

Where ρ is the density of the fluid, for seawater ρ = 1025 kg/m^3 , g is the gravitational acceleration (9.81 [m/s^2)] and h is the hight of the fluid, in this thesis the hight refers to the submerged depth. The equation will find the hydrostatic pressure at one point, not the pressure variation.

For water the variation is linear with respect to the depth, this is because the weight of the water is the only contributing factor. The linear variation per meter is, the derivative of the gage pressure, P_{gage}, in respect of the height, h [9]:

$$\frac{dP_{gage}}{dh} = -\rho g$$ *Eq. 2-21 Linear Variation of Hydrostatic Pressure*

2.5.2 Marine Environmental Loads

Environmental conditions cover natural phenomena which may contribute to structural damage. For a column-stabilized unit the suitability depends on the environmental conditions in the area of the intended operation. Usually, the unit is designed for either worldwide use or for a specific region or site. For column-stabilized units the following set of environmental phenomena are of general importance [10]:

- Waves
- Currents
- Wind
- Snow and ice
- Temperature
- Water depth

These phenomena have direct impact on floating offshore structure as well as in an indirect way as they are connected through a mooring system. These environmental phenomena will not be coved in depth in this thesis, as they are included in the displacement field applied to the local models. The displacement fields are a result from analysis of the global conceptual model given by Global Maritime.

The global model is designed according to the newest versions of:

- Rules for classification, DNV-RU-OU-0503, *Offshore fish units and installations*
- Recommended practice (RP), DNV-RP-C103), *Column-Stabilised Units*
- Offshore standard (OS), DNV-OS-C103, *Structural Design of Column Stabilised Units -LRFD Method*, (LRFD is Load and Resistance Factor Design)

The most significant environmental loads for the hulls of column-stabilized units are normally those induced by waves [11]. GM Aqua Design is designed to withstand a significant wave height, H_s, of 17.3 m for a return period of 100 years. The significant wave hight is the average of the third highest wave heights in a sea state with a duration of 3 hours. [11] For units intended for unrestricted service (worldwide) a maximum H_s of 17.3m will cover most locations. [4]

3 FATIGUE

Components subjected to time varying loads may be subjected to fatigue failure. Loads that vary over time are called dynamic loads. The variation can be in magnitude, direction, or application position or a combination of these. Fatigue failure occurs because of formation of cracks in a three-stage process [12].

- Stage I – formation of cracks (crack initiation)
- Stage II – crack growth (crack propagation)
- Stage III – fracture

3.1 Cyclic Loads

Cyclic loads are expected to vary throughout the lifetime of the structure. Wind and wave loads are examples of load types that have a cyclic load pattern. A cyclic load is usually defined by the stress amplitude, which is related to the stress range, σ_r, which is defined as the difference between the maximum, σ_{max}, and minimum stresses, σ_{min} [12].

$$\sigma_r = \sigma_{max} - \sigma_{min}$$ *Eq. 3-1 Stress Range*

The stress amplitude, σ_a is defined as half of the stress range [12]:

$$\sigma_a = \frac{\sigma_{max} - \sigma_{min}}{2}$$ *Eq. 3-2 Stress Amplitude*

3.2 Method of Fatigue Analysis

Fatigue analyses are commonly based on fatigue tests. During a fatigue test a test piece is subjected to constant amplitude stress cycle and then the number of cycles is counted, until fractures appear. If the test is repeated several times with different applied stress ranges, the results can be plotted in a graph. The number of cycles to failure, N, is plotted on the horizontal axis and the stress range, S on the vertical axis. The curves fitted to the datapoints from the fatigue testing are called S-N curves. The S-N curves for a range of different materials and environments exist today [12].

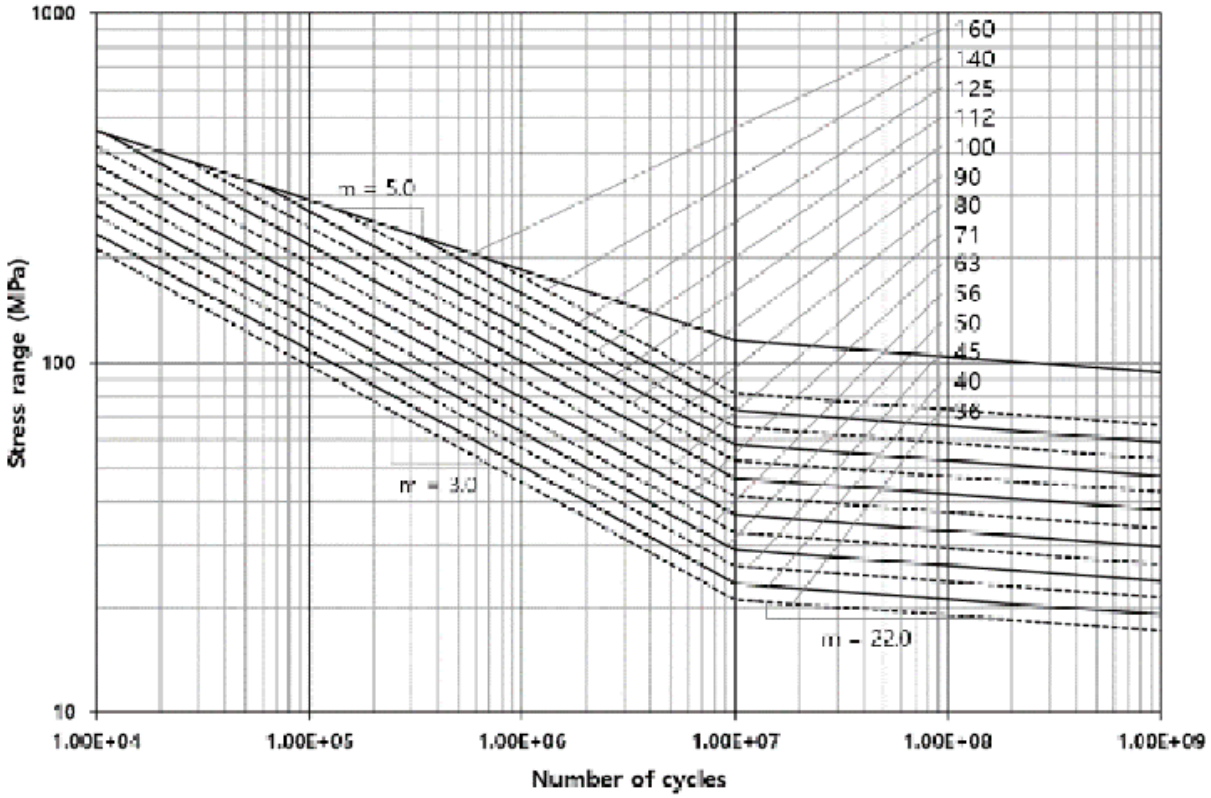

Figure 3-1 S-N curves for steel in air, from DNV-RP-203, [13]

3.3 High Cycle and Low Cycle Fatigue

Fatigue is usually divided in to two subtypes, high cycle and low cycle fatigue. High cycle fatigue occurs when the applied cyclical stresses are low and failure occurs after a large number of cycles, typically high cycle fatigue occurs after more than 10 000 cycles [12]. For example, wave actions show about $5 \cdot 10^6$ cycles a year [13]. Since the stresses are low only elastic deformation will occur [12].

Low cycle fatigue on the other hand occurs when the applied cyclical stresses are higher and occurs after a smaller number of cycles, usually less than 10 000. Due to higher stresses, plastic deformation can occur in addition to the elastic deformations. For low cycle cases a strain-based approach such as the Coffin-Manson relation is usually preferred [13].

3.4 Description of the Wave Pattern

The amplitude of a wave loading is non-constant. Loads with a non-constant amplitude are frequently called spectrum loading or irregular loading. Spectrum loadings can be generated by a random process, such loads are called random loading or stochastic loading. The stochastic loading is generated by an algorithm given a sequence of loading peaks and valleys. The cumulative effect of non-constant amplitude loads must be calculated. To calculate the cumulative effect the stress-time history is broken down into individual cycles, which are summed up to a distribution of stress ranges. There are several methods calculating this, one such calculation method is the linear damage hypothesis [12].

3.5 Linear Damage Hypothesis

The linear damage hypothesis also known as the Palmgren- Miner's Rule is used to calculate the total damage from varying cyclic loads. It states that the total damage, D, is equal to the sum of the damage fractions caused by each stress cycle [12].

$$D = \sum_{i=0} \frac{n_i}{N_i}$$

Eq. 3-3 Linear Damage Hypothesis

n_i is the number of cycles at a certain stress range, S_i, and N_i is the number of cycles to failure at stress range S_i. If $D \geq 1$ fatigue failure is assumed to have occurred [12].

3.6 Simplified Fatigue Calculation

This thesis does not include any calculations related to fatigue failure as it exceeds the limits of this thesis. However, since fatigue failure often is the governing load case for offshore structures, structural details that are at risk of fatigue failure will be highlighted in this thesis. Simplified fatigue calculations relate the principal stresses from dynamic load cases to fatigue failure. Areas with high stress concentrations are at risk of fatigue failure [13]: Such areas are often:

- Geometric discontinuity
- Welds
- Transition zones
- Holes and cut-outs

3.7 DNV-RP-C203

The recommended practice DNV-RP-C203, Fatigue Design of Offshore Steel Structures, is developed with the purpose of assessing high cyclic fatigue. “Fatigue analysis should be based on S-N data, determined by fatigue testing of the considered welded detail and the linear damage hypothesis.” [13] .

S-N curves for steel materials in air with yield strength less than 960 MPa as well as steel materials in seawater with cathodic protection and steel with free corrosion with yield strength up to 550 MPa can be found in DNV-RP-C203. The S-N curves steel in air is shown in Figure 3-1.

4 FINITE ELEMENT METHOD

4.1 Introduction to Finite Element Method

The Finite Element Method (FEM) is a method to solve partial differential equations (PDE) by finding approximate answers. The PDEs describe the laws of physics for space- and time- dependent problems and are hard to solve or cannot be solved, thus approximations are used. The approximations are constructed by different types of discretisation, causing finite elements (FE) connected through nodes, the collection of these nodes and FEs are called the mesh. The discretisation approximates the PDEs with numerical model equations, which can be solved using numerical methods and thus finding an approximate answer. Discretisation is one of the main steps in finite element analysis. These main steps are [14]:

1. Modelling
2. Discretisation of the model (meshing)
3. Element description
4. System description
5. Boundary and load definitions
6. Solving
7. Postprocessing, including evaluation of the results

The material and geometric behaviour of each element when subjected to loading is described by a structural matrix (step 3). There are two types of structural matrices, stiffness matrix and transfer matrix. The stiffness matrix correlates the forces to the displacements at the nodes, while the transfer matrix relates the forces and displacements of one node to another [15].

The stiffness matrix [k] and the displacement, {d} is related to the forces, {r} at the same node by the following element equation for each element. r^0 is the initial state of the node related to i.e., temperature or displacement [14], [15].

$$\{r\} = [k]\{d\} + \{r^0\} \qquad \textit{Eq. 4-1 Element Equation}$$

All the element equations should be assembled in order, to get the global system of equations of the system (step 4) [14]

$$\{R\} = [K]\{D\} + \{R^0\}$$

Eq. 4-2 Global system of element equations

[R] is the forces for the entire system, [K] stiffness matrix for the entire system and {D} is the displacement of the entire system. $\{R^0\}$ is the initial state of the system due to i.e. temperature or displacement [14].

The derivation of the stiffness matrices is not covered in this thesis as it is not the aim of this thesis.

4.2 Beam Elements

Beam elements are geometrically speaking the simplest structure used in finite element modelling. Beam elements should be long compared to their cross-sectional area and should undergo relative consistent bending, torsion, and/or compression [5]. A convenient way to think of beam elements is to think about the elements as providing the gross or general system performance information. [5]

4.3 Plate and Shell Elements

Plates are elements where the thickness is significantly smaller than the span in the other two dimensions and carries load perpendicular to the plane [16]. Plate theory is often regarded as an extension of beam-theory, in the sense that a beam is a 1D specialisation of a 2D plate. Plate theory differentiates between thin plate theory, thick plate theory and theory for 3D elements (volume elements). [14]

Volume elements are only used in special cases as they require the mesh to be verry fine to obtain accurate results. Two such special cases are especially thick plates and plates with areas subjected to critical stress concentration. [14] Thin plate theory is also known as Kirchhoff theory for plates and is equivalent to Euler-Bernoulli theory for beams. Thick plate theory is known as Mindlin theory for plates and is equivalent to Timoshenko theory for beams. [17]

The main difference between thin and thick plate theory is that thick plate theory includes transverse shear deformation in plate-bending in addition to bending deformation. This is a result of thin plate theory assuming that a vertical line remains straight and perpendicular to the neutral plane of the plate during bending. In contrast, thick plate theory only assumes that the line remains straight, it is no longer assumed to be perpendicular to the neutral plane. This difference is derived between Euler-Bernoulli and Timoschenko beam theory, in contrast to the plate theory the beam theory has a neutral axis instead of a neutral plane. [17] The difference between Timoschenko and Euler-Bernoulli is visualized in Figure 4-1 Euler- Bernoulli and Timoshenko beam.

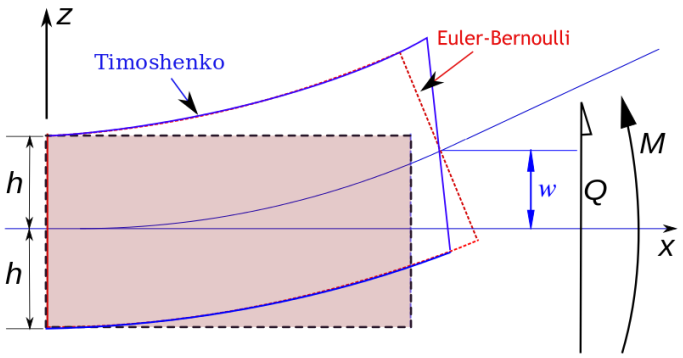

Figure 4-1 Euler- Bernoulli and Timoshenko beam, [22]

Thick plate formulation is recommended in general, but some specific examples are [14]:

- Cases where shear deformation can become significant.
    - Locations with significant bending-stress concentrations, such as areas with sudden changes in thickness or support conditions and near openings and corners.
    - For curved shells.
- Stiffness tends to be more accurate, if the mesh is adequate.
    - Adequately meshed thick shells tend to be more flexible than thin shell, due to the inclusion of shear deformation.

Thick plate formulation is not recommended in cases where shear deformations are known to be small as the accuracy of thick plate formulations is sensitive to mesh distortion. If the mesh is too coarse the element can become too stiff. It is important to use an adequate mesh when using thick plate formulation. [14]

4.4 Meshing in Finite Element Analysis

Meshing is one of the most important steps in finite element analysis, because the quality of the finite element result depends on the quality of the element mesh. Finding the most optimal mesh can be tricky as the answer depends on the structure configuration as well as the complexity of the loads. Therefore, it is important for the user to be able to adjust the mesh as needed. Important adjustments include [18]:

- Number of finite elements, density of the mesh
- The shape of the finite elements
- The type of finite element, I.e. First, second or higher order
- Meshing algorithms
- Mesh priorities, meshing all in one go or specifying a sequence on meshing the structural parts
- Different mesh densities can be needed for various structural parts or load patterns.

4.4.1 First and Second Order Elements

As mentioned, it is important to choose the most optimal type of element. The two main types of elements are first order elements and second order elements. Higher order elements exist but will not be discussed in this thesis as GeniE only separates between first and second order type elements [19]. The main difference between a first and second order element is that a first order element only has corner nodes, while a second order element has mid-side nodes in addition to the corner nodes. A first order element is shown in Figure 4-3 and a second order element is shown in Figure 4-2The corner nodes are shown in black for both figures, while the mid side nodes are shown in grey for the second order element. This means that second order elements can have curved edged while first order element must remain straight. There is also a difference in the behaviour of the polynomial functions. These

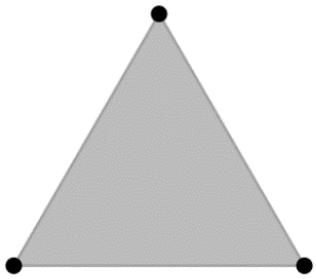

Figure 4-3 First order element

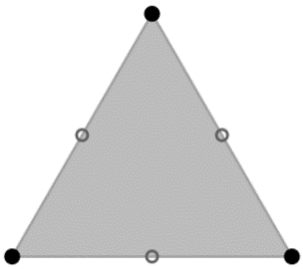

Figure 4-2 Second order element

functions are called shape functions or interpolation functions. Shape functions interpolates the solutions obtained at the nodes. For first order elements shape functions are linear (first order) while they are quadratic (second order) for second order elements [16].

The shape functions for 1D elements, such as beams are [16]:

$$Linear\ (first\ order): P(x) = a \cdot x + b$$ *Eq. 4-3 1D First Order Element*

$$Quadratic\ (second\ order): P(x) = a \cdot x^2 + b \cdot x + c$$ *Eq. 4-4 1D Second Order Element*

The shape functions for 2D elements such as plates are [16]

$$Linear\ (first\ order): P(x) = a_1 \cdot x + a_2 \cdot y + a_3 \cdot x \cdot y + b$$ *Eq. 4-5 2D First Order element*

$$Quadratic\ (second\ order):$$

$$P(x) = a_1 \cdot x + a_2 \cdot y + a_3 \cdot x^2 + a_4 \cdot x \cdot y + a_5 \cdot y^2 + a_6 \cdot x^2 \cdot y + a_7 \cdot x \cdot y^2 + b$$

Eq. 4-6 2D Second order elements

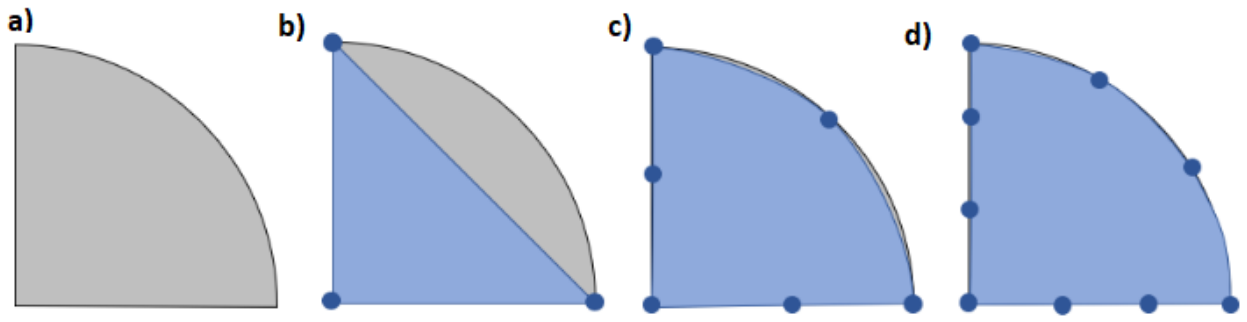

Figure 4-4 Higher Order Elements

Figure 4-4shows the same domain, a quadrant (figure a)) , discretised with three distinct functions. In b) the quadrant is discretise using a linear shape function, in c) a quadratic shape function is used and in d) a cubic function is used. The curved boundary in b) is quite poorly represented by the linear function, while the straight edge of the domain is represented precisely. The quadric function gives a better representation of the domain, figure c). The cubic shape function (third degree element) shown in figure d) gives an even better representation of the curved boundary.

If nodes were added to the curved boundary in figure b) a linear shape function would give a better representation than shown in figure b, but this also means that the number of elements will increase. This improved representation is visualised in Figure 4-5 with, 1, 2 and 3 elements.

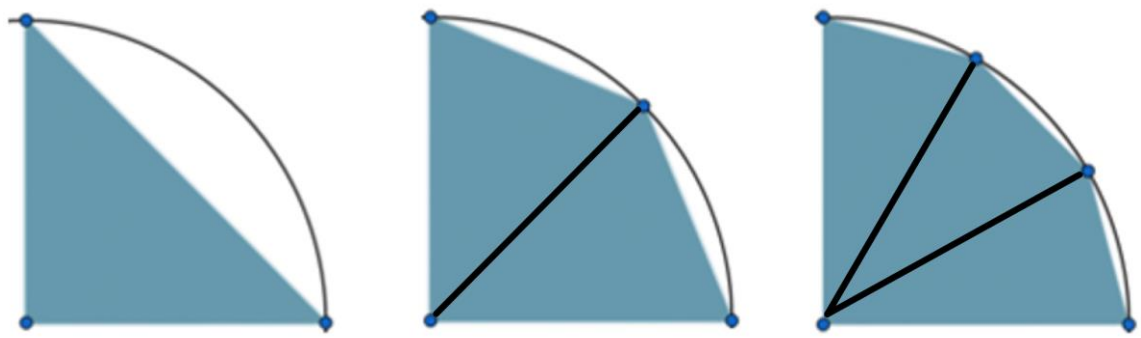

Figure 4-5 First order element partition

Elements of second order are used to get more accurate deformations and better geometric representation but are computationally expensive and inefficient compared to first order elements. Second order elements can cause a more realistic deformation with fewer elements because they are able to have curved edges as well as the quadratic polynomial functions. This is shown in Figure 4-5.

4.4.2 Isoparametric elements

The term isoparametric is derived from the prefix iso- meaning equal and refers to the use of the same shape functions to define the element's geometric shape as is used to define the displacements within the element. [14] Isoparametric formulation will ensure compatibility between neighbouring elements. The term compatibility in material refers to a material that is continuous as it deforms, and adjacent sections will share deformations. [16] This ensure that no material gaps or overlapping appear as the material deforms.

4.4.3 Convergence

Convergence is the process of successive mesh refinement to produce the optimal mesh [5]. Finding the optimal mesh is important to capture the behaviour of the system. The importance of the mesh is based on the importance of accurate results. An accurate solution is defined by Adams and Askenazi as "(…) the best solution to the geometry, properties, and boundary conditions presented." [5]. They also mention that accurate result depends on the degree of confidence of other assumptions made referring to the four primary assumptions in FEA design.

The four primary assumptions are geometry, properties, mesh, and boundary conditions [5]. Some of the assumptions made for a linear static analysis are mentioned in more detailed in chapter 2.2 Linear Static Analysis. The mesh must represent the physical model and its behaviour under loading in an acceptable manner.

Finding the right relationship between the accuracy and complexity is an important aspect of FEA. As mentioned, higher order elements are more computational expensive, but will converge faster (less elements). The size of the stiffness matrix for an element (and thus also the system) will increase with the order of the element. Performing a convergence analysis will ensure an accurate result, in the shortest amount of time.

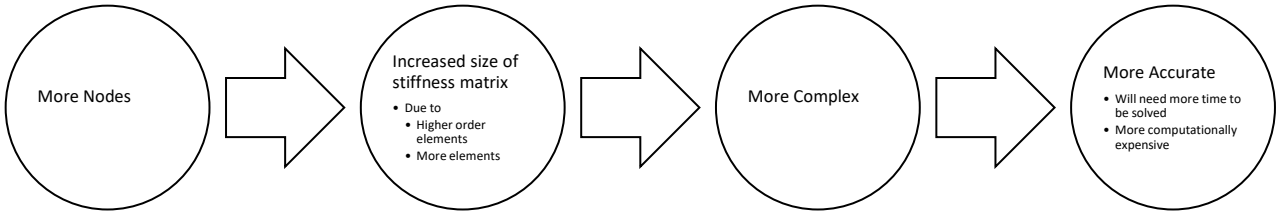

5 SESAM SOFTWARE AND SESAM GENIE

Sesam is a software developed for structural and hydrodynamic analysis of offshore structures and ships. It is based on the displacement formulation of finite element (FEM) [19]. GeniE is one of several Sesam modules. Other modules include Wajac and Wadam. Sesam Manager is a control module that can set up runs in the different Sesam modules. An overview of the modules is shown in Figure 5-1 Sesam Overview. The modules used in this thesis are marked with red circles in the same figure. [19]

GeniE is a tool for concept (high level geometry) modelling of beams, flat plates, and stiffened shells. It has several load modelling types including equipment (with automatic load transfer), explicit loads (point, line, and surface), and wind loads. Models made in GeniE can be transferred to other modules for further analysis, such as Sestra for structural and dynamic analysis and to Wajac and Wadam for hydrodynamic analysis. The results from Sestra can be postprocessed in Xtract [19].

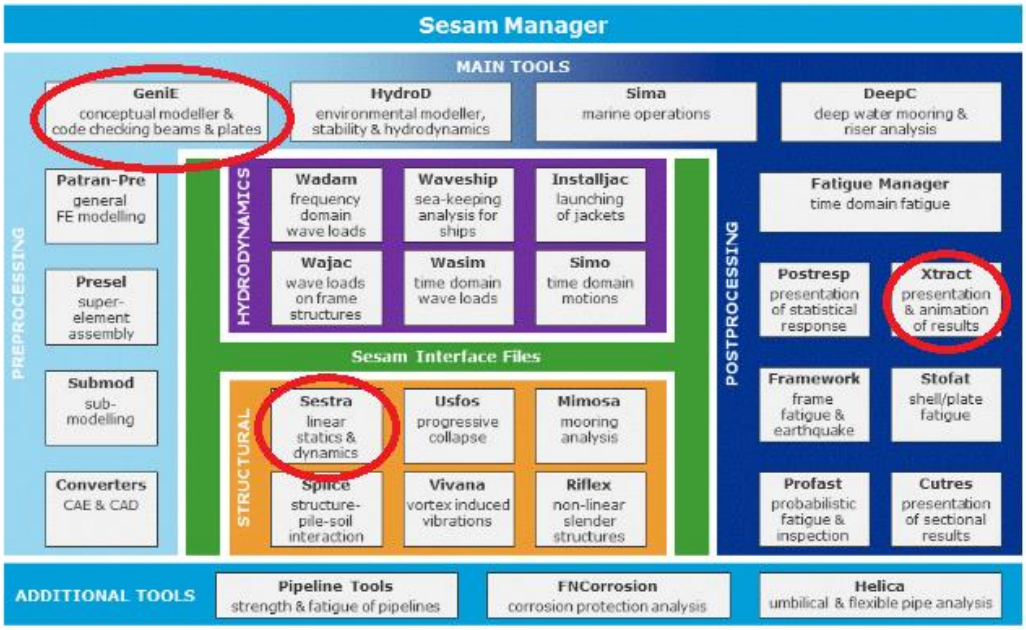

Figure 5-1 Sesam Overview, [19]

5.1 GeniE

The feature descriptions given in this section are based on the descriptions given in *FEATURE DESCRIPTION Sesam Software suite for hydrodynamic and structural analysis of renewable, offshore, and maritime structures from DNV* [19] and from *SESAM USER MANUAL GeniE – Vol 3 – Modelling of plate/shell Structures.* [18]

5.1.1 Meshing in GeniE

GeniE does not have a default mesh setting that will guarantee the optimal analysis result, but it has a default setting. By default, GeniE will mesh all in one go, use as large FEs as possible and create first order elements [18]. The meshes created in GeniE also reflects the basic geometry of beams, plates, and shells and the mesh points (nodes) will be where the geometry intersects. [19] The adjustment mentioned in section 4.4 Meshing in Finite Element Analysis are possible to make in GeniE

The mesh density is determined by two mesh properties in GeniE. Either by specifying the length of the elements edge or by the number of elements along a line or plate edge. Various parts of a model can have different densities. If a structure has different mesh densities for various parts, there will be a transition zone between the fine and coarse mesh. GeniE will by default make this transition zone as short as possible, but the user can extend the zone by specifying a growth rate for the mesh density [19].Fine meshing is beneficial in areas with large gradients, joints can be such a location.

The user can create any number of priority levels in GeniE, so that the meshing of important parts can be prioritized in the order the user wants. I.e., The important parts are meshed first (priority 1) and the less important parts after that [19].

5.1.2 Finite Element Types in GeniE

Models as well as parts of it, can be meshed using a range of different beam, plate, and shell element types. GeniE distinguishes between first and second order elements and create the following finite element (FE) types [19]:

- Truss, Including tension-only and compression-only
- Two node beam, can be hinged
- Two node spring and damper
- Three node beam (GeniE term: second order)

- Three node triangular flat plate
- Four node quadrilateral flat plate
  - For the flat plates three additional versions are available
    - Membrane, i.e. no bending stiffness
    - With drilling degree of freedom
    - With improved description of thick shell behaviour

- Six node triangular curved shell (GeniE term: second order)
- Eight node quadrilateral curved shell (GeniE term: second order)
  - Membrane versions of the two curved shell elements exist.

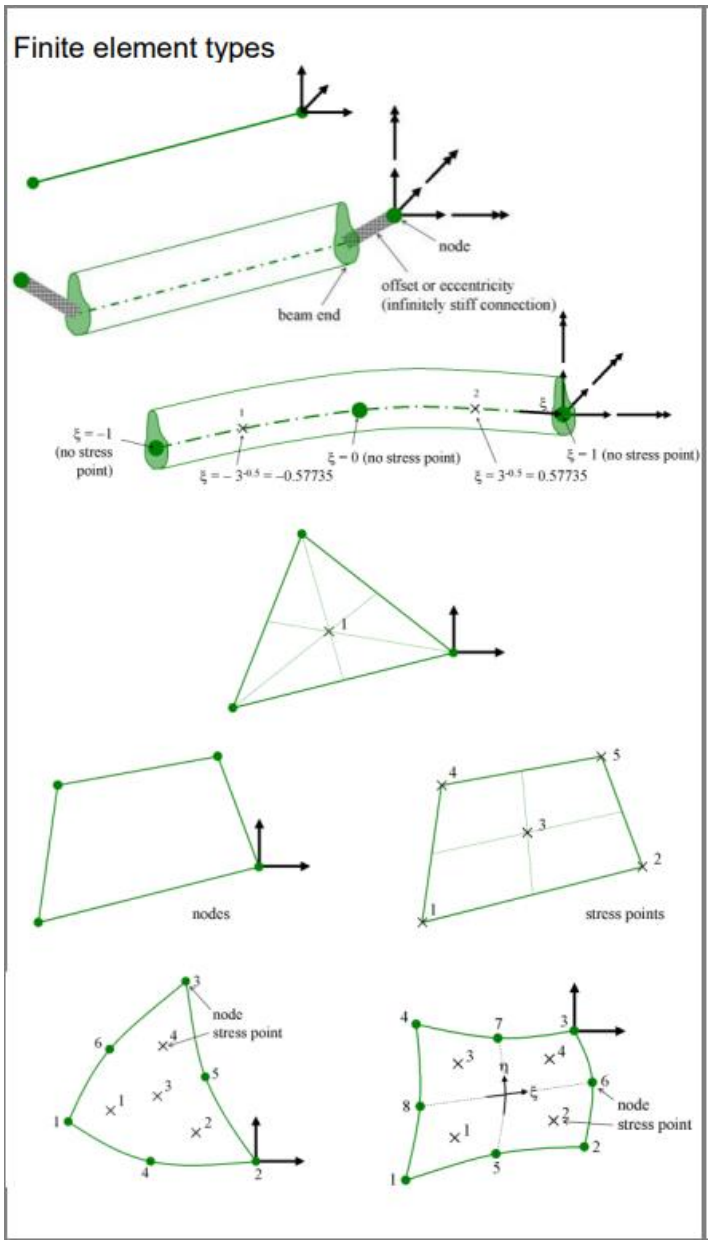

Figure 5-2 Element types used in GeniE, [19]

The finite element types listed are shown in Figure 5-2 Element types used in GeniE and Table 5-1 Element types in GeniE .

Name	Type	Order	Comments
2-node beam element	BEAS	1st	
3-node beam element	BTSS	2nd	Straight beams can be used in code checking
Triangular flat thin shell element	FTRS	1st	
Quadrilateral flat thin shell element	FQUS	1st	Inserted when adjusting mesh rules to split elements
Quadrilateral sub parametric curved thick shell element	SCQS	2nd	
Triangular sub parametric curved thick shell element	SCTS	2nd	Inserted when adjusting mesh rules to split elements
Quadrilateral flat thin shell with drilling dof	FQAS	1st	Includes the rotational dof around the axis perpendicular to the membrane in the membrane formulation
Triangular flat thin shell with drilling dof	FTAS	1st	- o -
Non-structural 2 node beam element	BEAS	1st	Special variant of BEAS with no contribution of the structural stiffness
Truss element	TESS	1st	Element type with no bending stiffness
Spring to ground	GSPR	1st & 2nd	Includes the 6x6 matrix
Shim element	GLSH	1st & 2nd	Special variant of the 2 node spring element with equal stiffness in two translation directions. No stiffness in other directions.
One node mass element	GMAS	1st & 2nd	May be eccentric if connected to a finite element node with 6 dof.

Table 5-1 Element types in GeniE, [19].

5.1.3 Meshing Algorithms in GeniE

There are two meshing algorithms supported by GeniE. Quad meshing algorithm (the Sesam quad mesher) and advancing front mesher (paver meshing). Quad meshing gives the best mesh in the middle of the surface and is intended for regular structures like topsides and rectangular parts. The advancing front mesher gives the best mesh along the edges and is thus best for details and irregular structural parts such as joint. These meshing algorithms can be combined in the same model [19].

5.1.4 Controlling the Mesh Quality in GeniE

In addition, GeniE has built in control mechanisms, where the user specifies the relevant check parameters if the user wants to over-ride the default settings. The user can also use its own experience or calibration studies [18].

5.1.5 Code checking in GeniE

GeniE supports several standards for member and tubular joint checking. Including EUROCODE onshore standard (EUROCODE 3), ISO offshore standard (ISO 19902 2007- offshore structures) and NORSOK, offshore standard (NORSOK 2004 and 2013) [18].

5.1.6 Guiding geometry in GeniE

Guiding geometry is used in GeniE to build on existing snap point. Available guiding geometry is for example guiding planes, guiding lines/curves and guiding points. Snap points can be used to find vectors and coordinates in the graphical window. For example, can a beam be inserted by clicking on two different snap points, a vector can be found in the same way [19].

6 MODELLING

6.1 Detailed Description of the Situation

The two models are based on two conceptual designs from Global Maritime. At the time of writing limited fabrication drawings were available, thus the modelling is based on the conceptual 3D-models from GeniE used to perform the global analysis. The conceptual GeniE-models are not fully analysed and thereby stiffener arrangement are missing.

The fish farm is a square construction, measuring 100m x 100m. The submerged part of the fish farm, shown in Figure 6-1, has four equal joints located at each corner, however only one is partially modelled. Each modelled joint consists of a column with a hight of 40 meters measured from the bottom plate (length a) and two pontoons that extend 40 meters from the centre of the column (length b). The bottom plate is located at 55 meters depth and thus all the modelled parts are submerged.

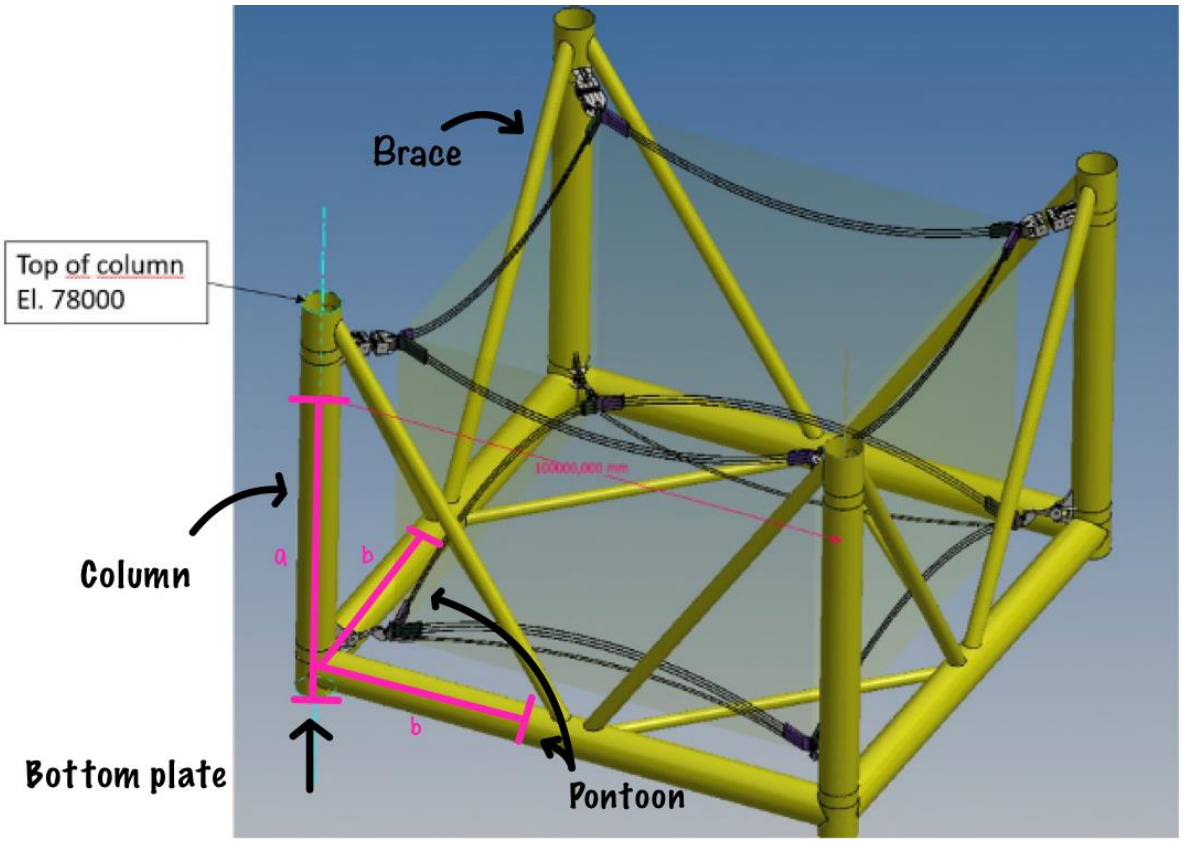

Figure 6-1 Submerged part of the fish farm

6.2 Units and Properties

The standard units set in GeniE are newtons, meters, and degrees Celsius.

6.2.1 Plate thickness

Both models are modelled using plates of thickness 35 mm. All the plates are of the same thickness.

6.2.2 Material

Both models are made of the same material, steel. The steel type used is S355 and is also called this in GeniE. The material properties are given in Table 6-1.

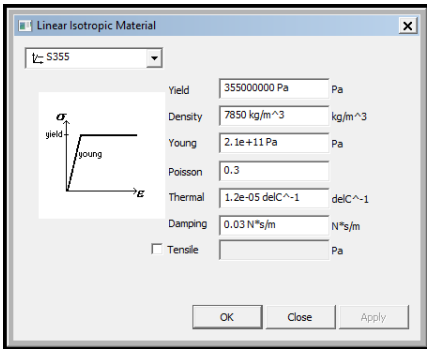

Figure 6-2 Material Properties

Table 6-1 Material Properties

Material Properties

Material	Description	Yield strength [MPa]	Density [kg/m^3]	Young's Modulus [GPa]	Poisson ratio
S355	Linear isotropic	355	7850	210	0.3

6.3 Geometry of The Models

The joints main parts are a column, two pontoons and a transition zone connecting these three elements. The column and the pontoons have a main diameter of 7m. The main difference between the two models is the transition zone of the joint where the column and the pontoons are joint together. One of the models have a conic transition zone and is called the conic model in this thesis. While the other one has a boxed transition zone, called the box model in this thesis.

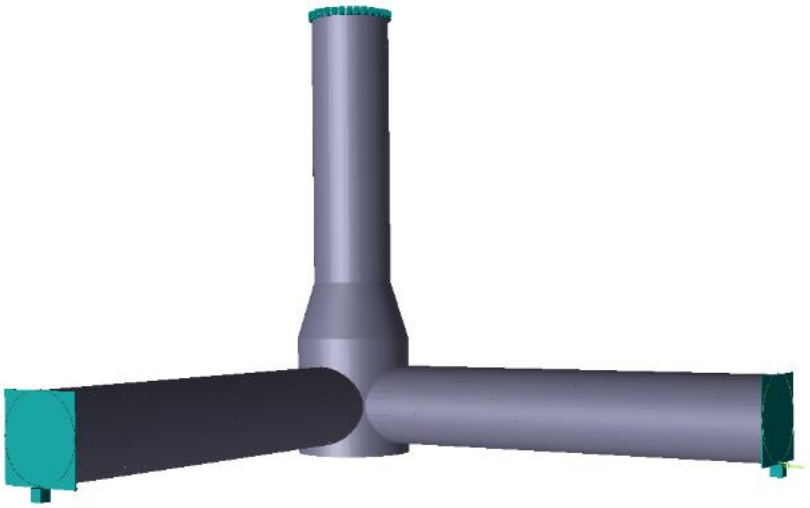

Figure 6-3 The conic-model

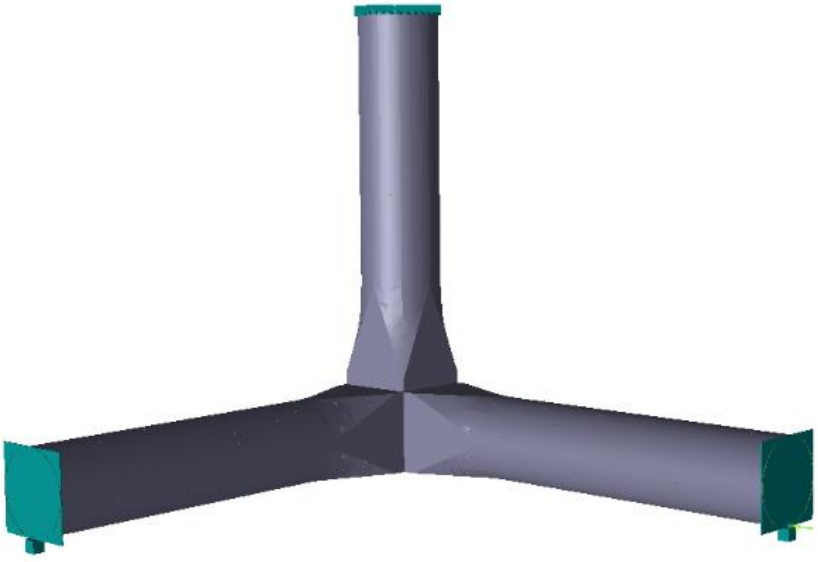

Figure 6-4 The box-model

6.4 The Conic Model

The conic-model's column has a wider bottom part with a diameter of 10.1 m and a hight of 10.5 m. The pontoons are connected to this bottom part. The bottom shell of the pontoon is elevated 1 meter above the bottom plate. The bottom part of the column extends 2.5 meters above the top shell of the pontoon with a diameter of 7 meters (1+2.5 +7=10.5). The model has a conic transition between the wider part and the rest of the column with a diameter of 7m. The conic transition part has a hight of 5 meters.

6.4.1 Guiding geometry

The main guiding geometry is a guiding plane. The guiding plane's origin is set to be at the centre of the fish farm. The grid is distanced so that it matches with the radii of the column, thus these are set to be 3.5m and 5.05m (3.5m + 1.55m). Guiding curves are used to make the main shell dimensions.

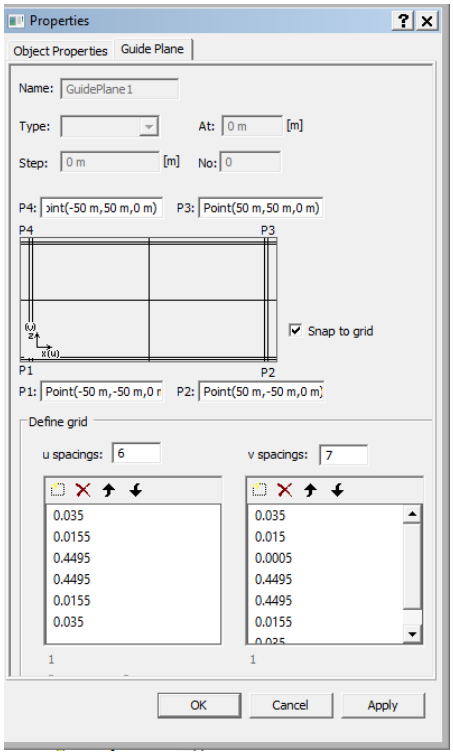

Figure 6-5 Guiding plane, conic-model

6.4.2 The internal structure

The internal structure consists of ring/frame stiffeners and longitudinal stiffeners. The stiffeners are modelled using beams of different sections. Since the cross-sectional area of the stiffeners is small relative to the length of the stiffeners, beam elements can be used. This will reduce the number of shell elements and the total number of degrees of freedom needed in the model, and thereby reduces the total computation time and power.

The longitudinal stiffeners are two different L-Sections, L370x13 and L100x8. Usually bulb flats are used, but since it is impossible to model bulb flats in GeniE equivalent L-profiles are used. The ring/frame stiffeners are two different T-sections, T1000x250x22x25 and T250x150x10x15.

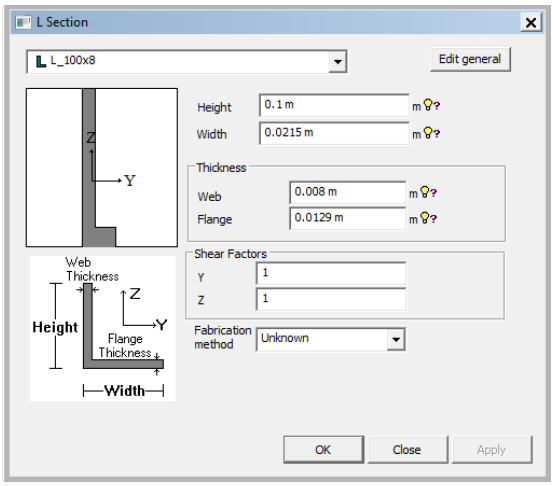

Figure 6-6 L100x8

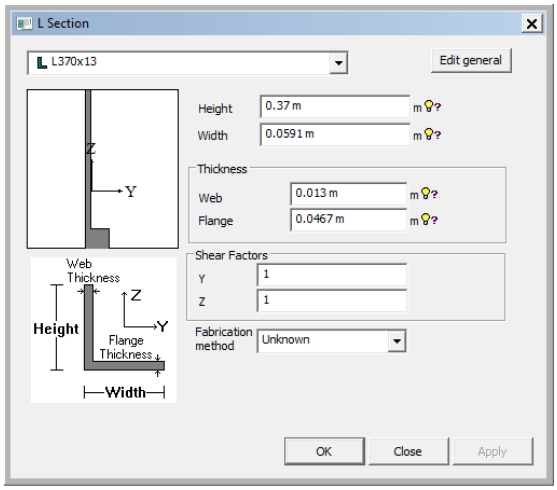

Figure 6-7 L370x13

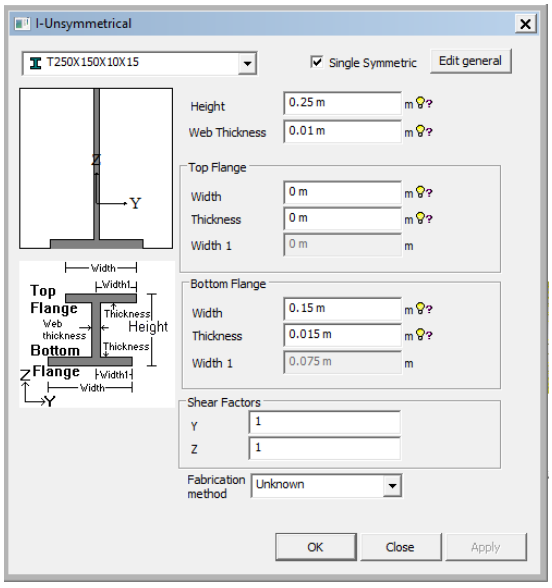

Figure 6-8 T250x150x10x15

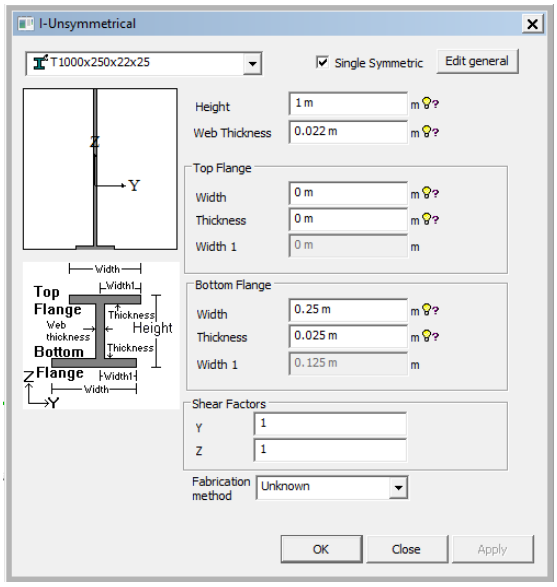

Figure 6-9 T1000x250x22x25

The arrangement of the different beam sections is shown in the figures below. Each section type is color-coded in the figures.

- L100x8 shown in pink was used as:
  - Longitudinal stiffeners in the top part of the column spaced 15° apart, totally 24
  - Longitudinal stiffeners in the pontoons spaced 10° apart, totally 36.
- L370x13 shown in lime green was used as:
  - Longitudinal stiffeners in the bottom part of the column spaced 10° apart, totally 36.
- T250x150x10x15 shown in turquoise was used as:
  - Ring stiffeners in the top and bottom part of the column and in the pontoons, spaced 2.5 meters apart. Except for the ring closes to the bottom plate in the column where the ring is located 2.535 meters from the bottom plate, hight h. The ring in the pontoons closes to the column is located 1.25m from the outer shell of the column, length b.
- T1000x250x22x25 shown in dark blue was used as:
  - Frames in the bottom part of the column and longitudinal stiffeners of the bottom plate spaced 1.7m apart

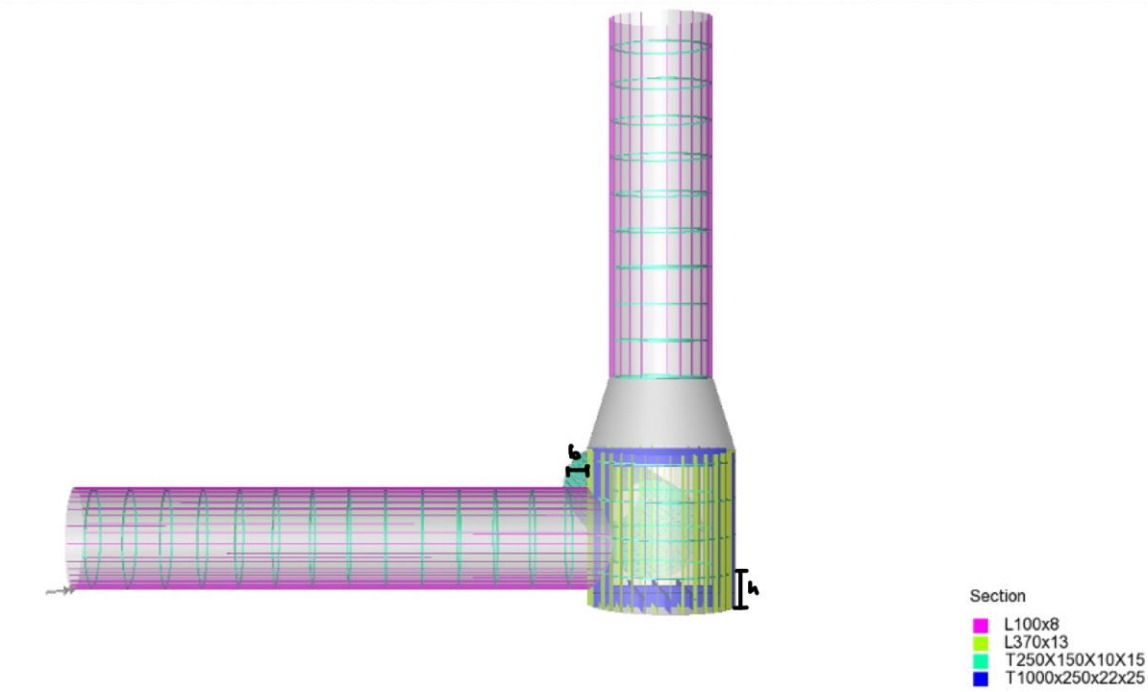

Figure 6-10 Internal beam arrangement in the conic-model.

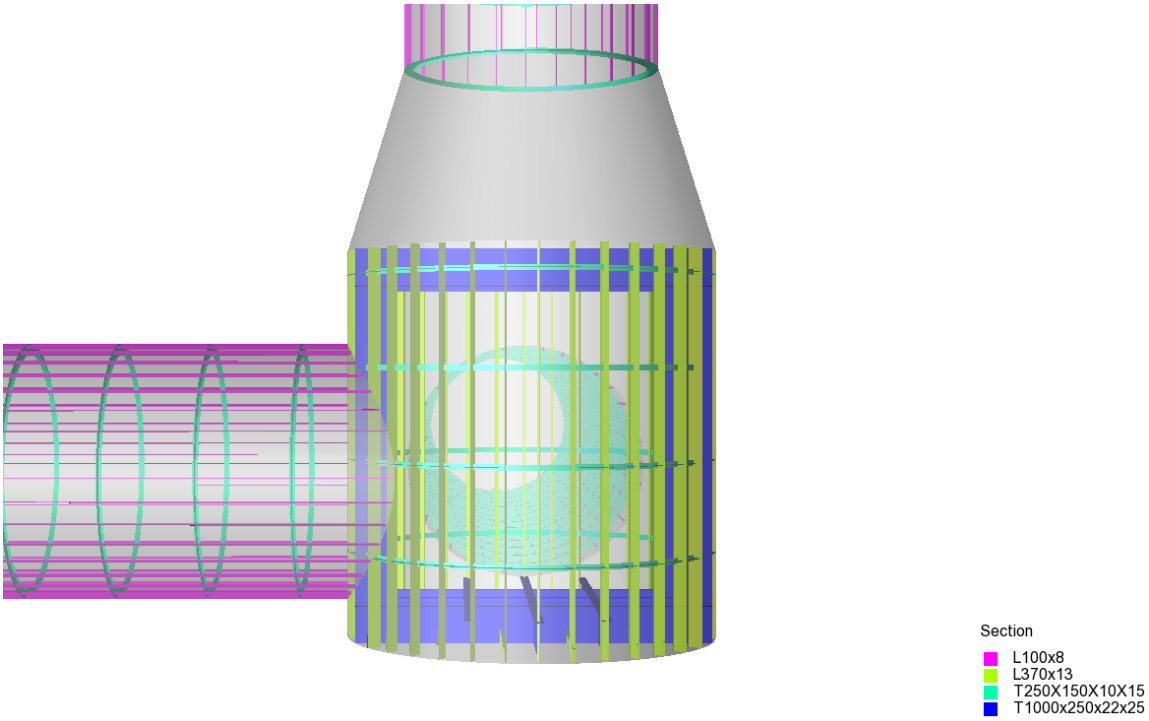

Figure 6-11 Beam arrangement, bottom of cylinder in conic-model

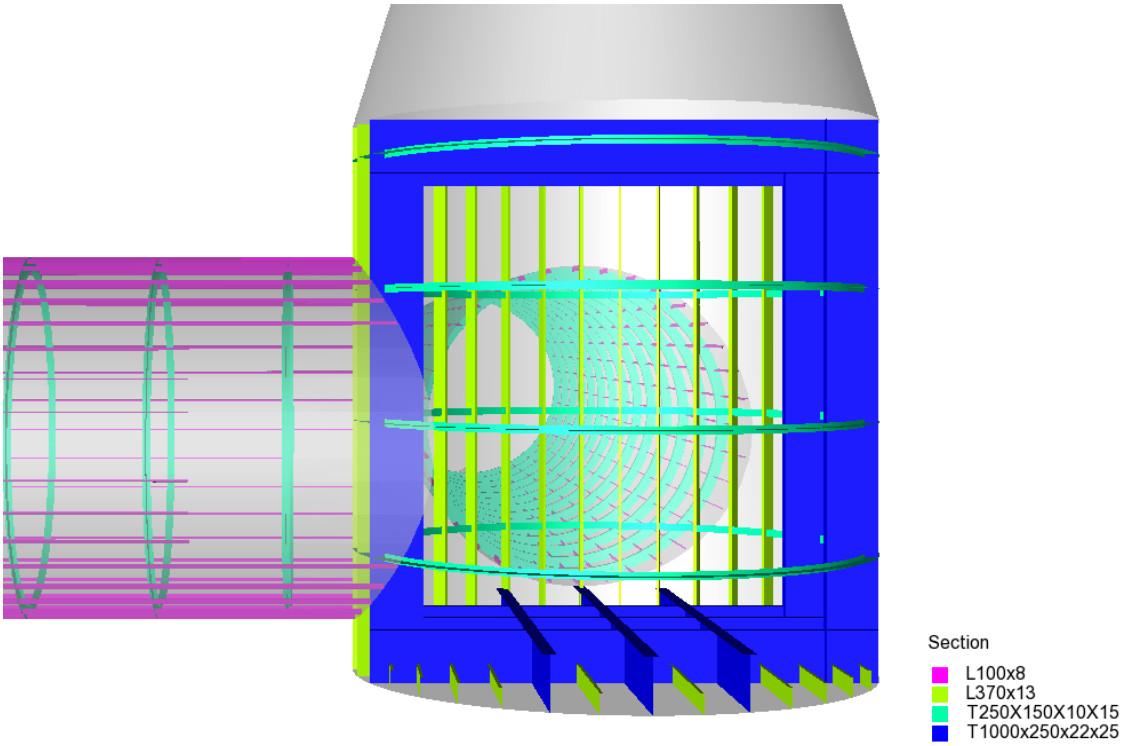

Figure 6-12 Frame in conic-model

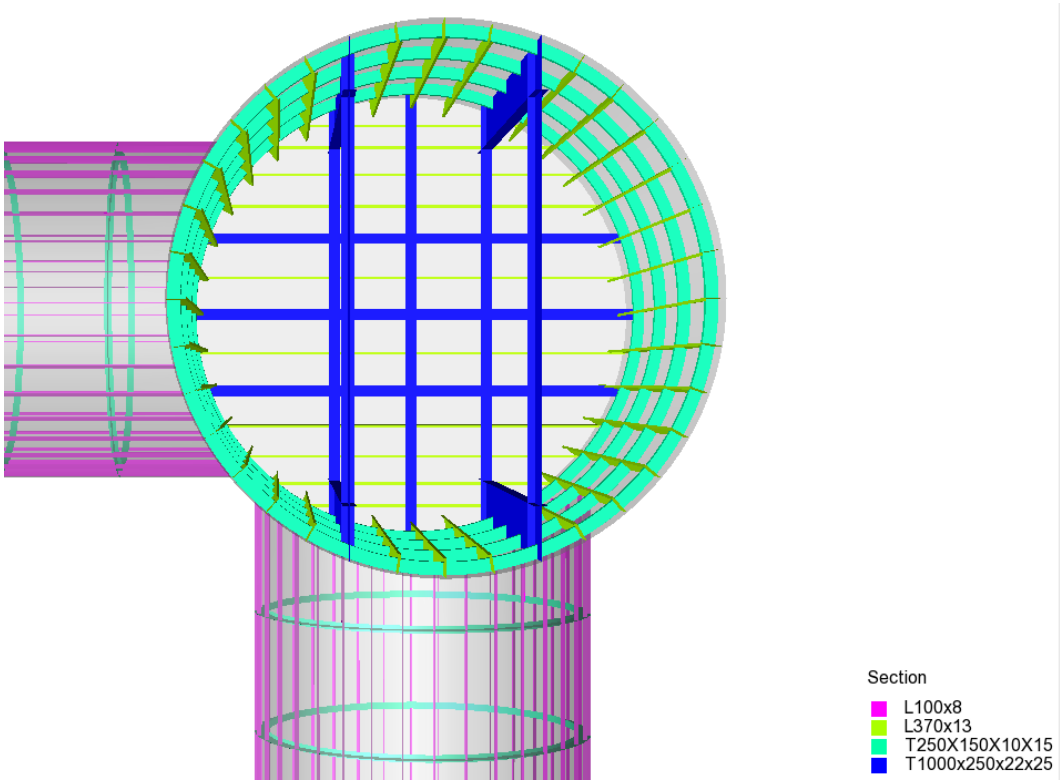

Figure 6-13 Internal arrangement top view of column, conic-model

6.4.3 Wet Surface

A wet surface called WS1 was made for the model, this wet surface is shown in blue in Figure 6-14 Wet surface of conic-model. The wet surface is used to apply a surface load corresponding to the hydrostatic pressure on the outer shell (the shell exposed to water). Since the entire model is submerged, the wet surface cover all outer surfaces including the bottom plate.

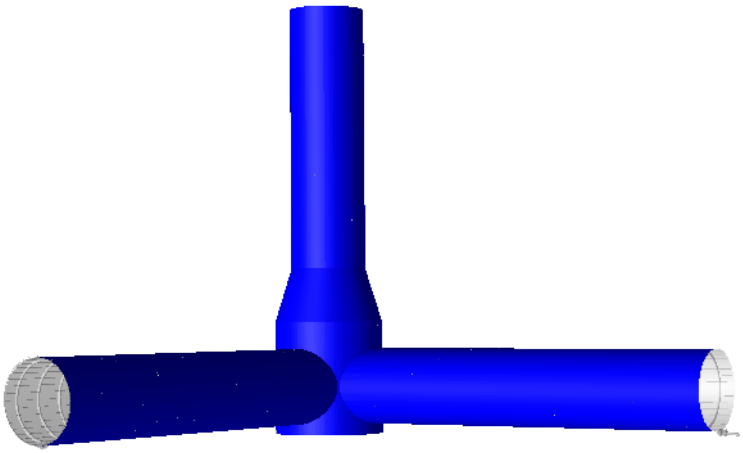

Figure 6-14 Wet surface of conic-model

6.5 The Box-Model

The column in the box model has a cubic bottom part (a box) measuring 7x7x7 meters. These measurements are a result of the diameters of the pontoons and column which are 7 meters too. The box has a one-meter extension-zone. The edge of the extension zone is connected to the pontoons and the column using triangular plates causing a transition zone to form the connection between the square shaped extension and the circular pontoons/column. The transition has a length of 8 meters.

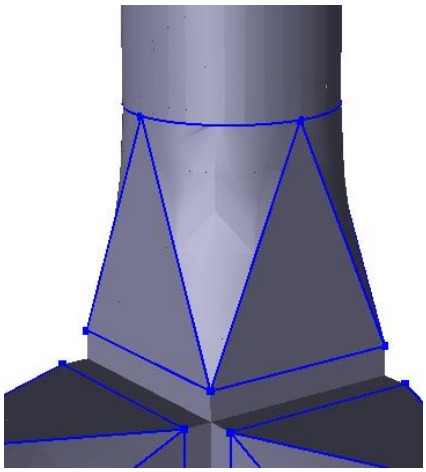

Figure 6-15 Transition zone, box-model

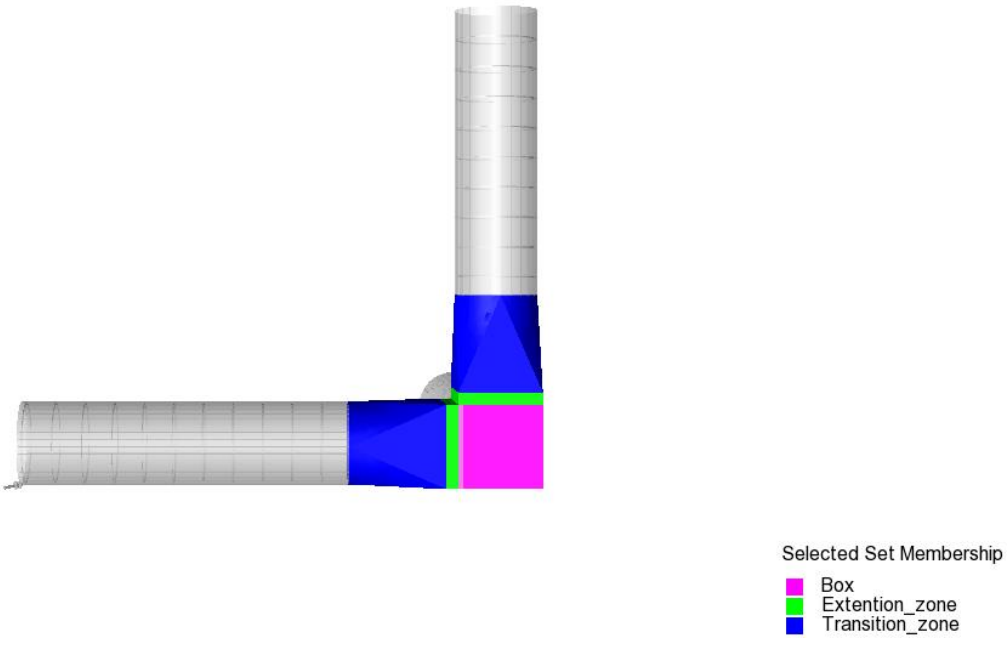

Figure 6-16 Terms used to describe the box-model

6.5.1 Guiding Geometry

The main guiding geometry for the box model is also a guiding plane, where the origin of the plane is set to be at the centre of the fish farm. The grid is distanced so that it matches with the radius of the column and pontoons (3.5 meters).

Guiding curves are used to make the main dimensions of the shell structure, as well as to make the triangular transition plates from the square box to the circular pontoon. The guiding curves are shown in blue in Figure 6-15.

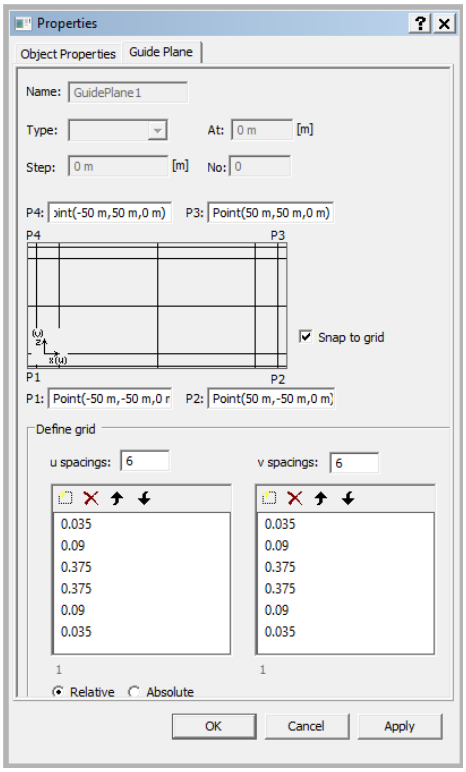

Figure 6-17 Guiding plane, box-model

6.5.2 Internal structure

The internal structure of the two models is made as similar as possible. In addition to the sections used in the conic-model T650x200x15x25 is implemented.

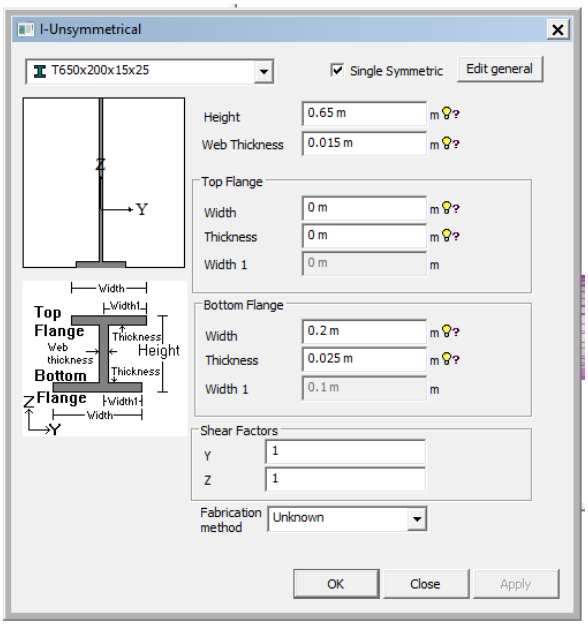

Figure 6-18 T650x200x15x25

The arrangement of the beam sections are shown in the figures below:

- L100x8 is pink shown in pink
  - Longitudinal stiffeners in the top part of the column spaced 15° apart, totally 24
  - Longitudinal stiffeners in the pontoons (spaced 10° apart, totally 36)
- L370x13 is shown in yellow
  - Longitudinal stiffeners in the box spaced 0.78 meters apart, totally 36
- T250x150x10x15 is shown in green
  - Ring stiffeners in the column and box and in the pontoons, spaced 2.5 meters apart
  - Ring stiffeners partially used in the transition zone between the box and the pontoon/column spaced 0.945 meters apart.
- T1000x250x22x25 is dark blue
  - Frames in the box (spaced ca.0.78m apart)
- T650x200x15x25 – light blue-
  - Ring stiffeners in the transition zone from the box to the pontoon, spaced 0.945 meter apart

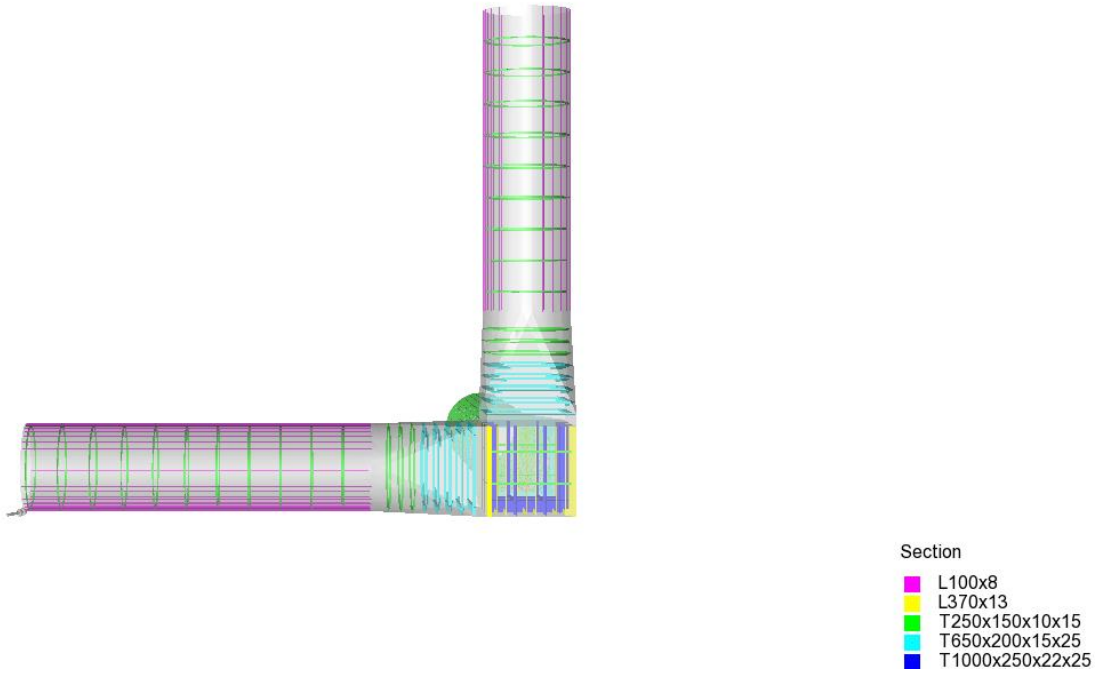

Figure 6-19 Internal structure arrangement, side view of the box-model.

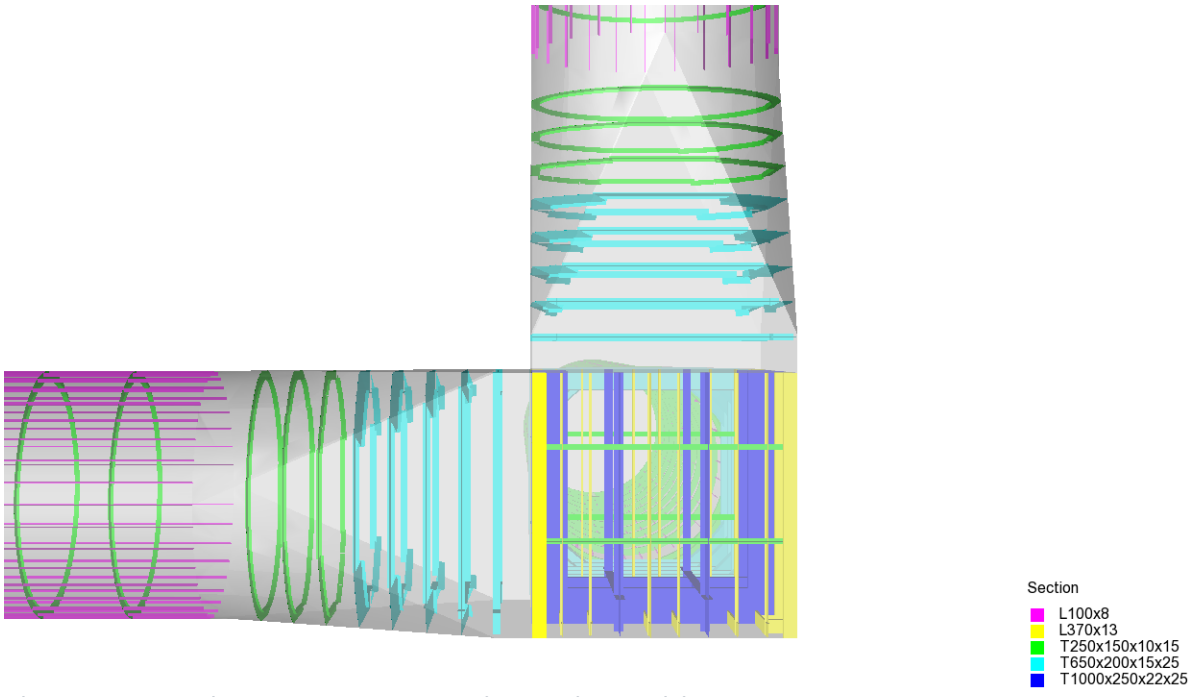

Figure 6-20 Internal structure arrangament, close up, box-model

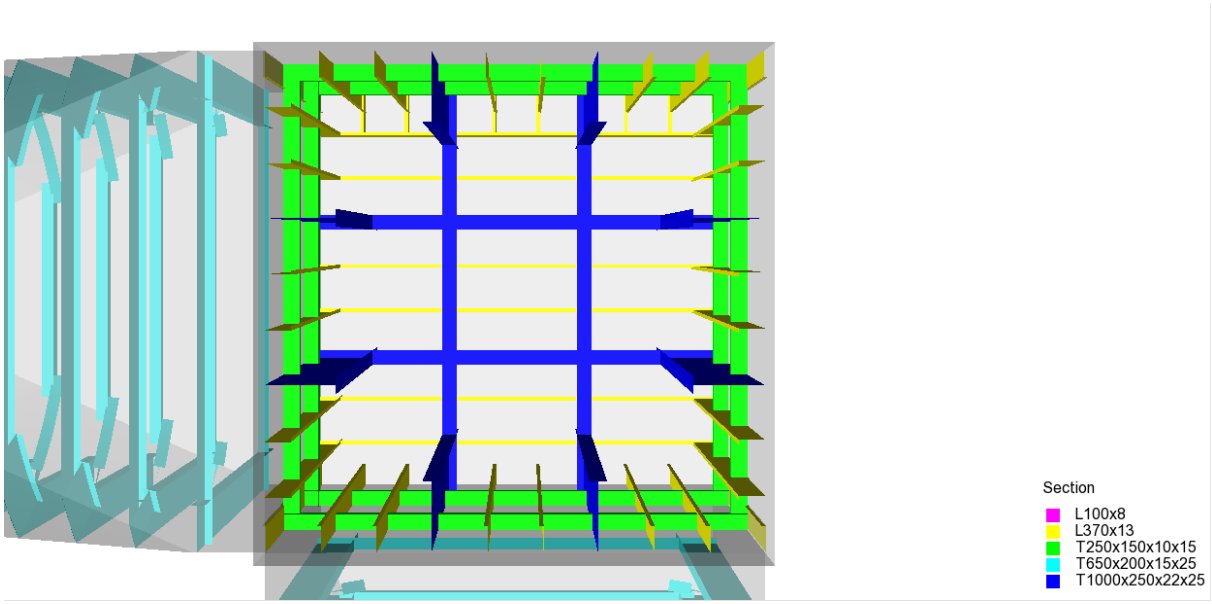

Figure 6-21 Internal structural arrangement, top view of box.

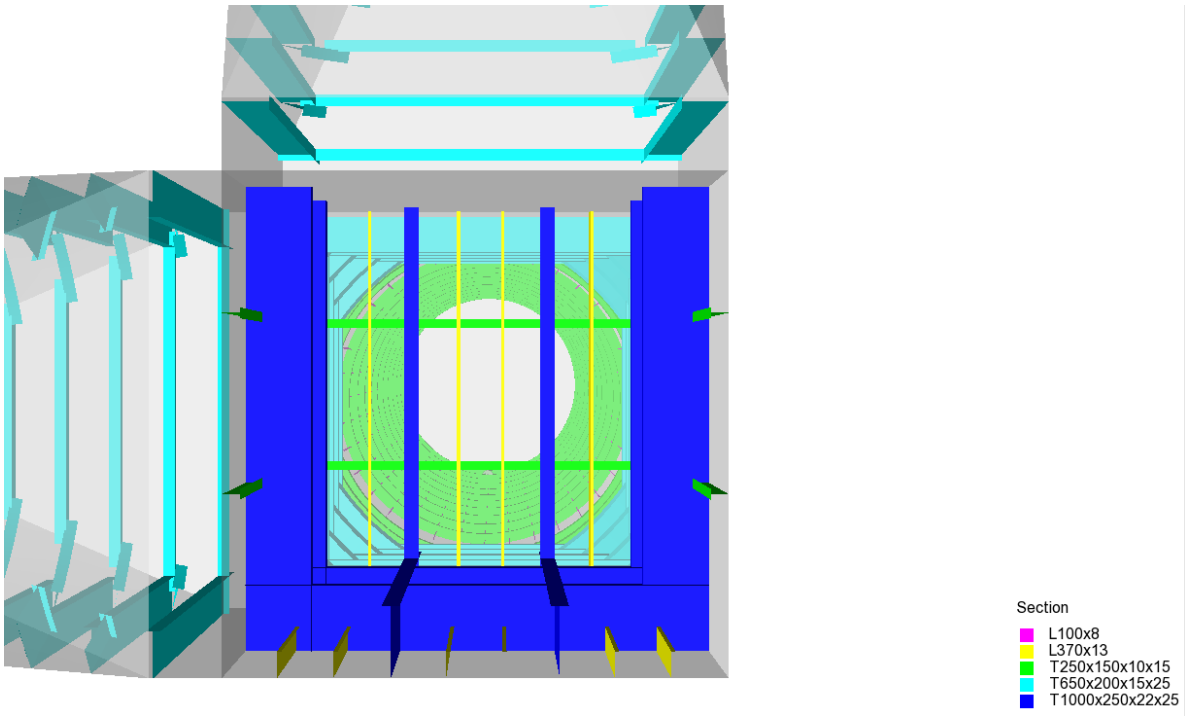

Figure 6-22 Internal structural arrangement, side view frame in box.

6.5.3 Wet Surface

The wet surface for the box model is shown in blue in Figure 6-23 Wet Surface of the box-model. This surface is used to apply a surface load corresponding to a hydrostatic pressure to the joint. The hydrostatic pressure is described in section 7.3 Loads.

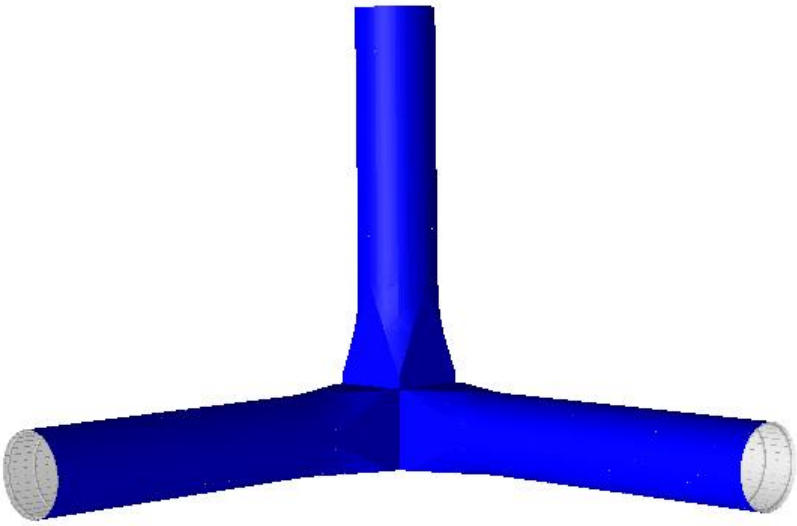

Figure 6-23 Wet Surface of the box-model

7 ANALYSIS

The analysis type used in this thesis is the linear static analysis. The analysis is running Sestra.

7.1 Meshing

The model has two different mesh densities, a finer mesh density, called Md_fine and a coarser mesh, called Md_ coarse. Md_fine is applied in the transition zone of both models as higher stress concentrations are expected here. Md_coarse is applied to the ends of the pontoons and column as lower stress constrations are expected here. Md_fine has an element size of 0.1 meters and Md_coarse has an element size of 0.75 meters, a growt rate of 1.05 causes a gradual transition between the fine and coarse mesh. The distribution of Md_fine and Md_coarse is shown in Figure 7-1 Mesh Distribution Conic Model and Figure 7-2 Mesh Distribution Box-Model. - Md_ fine is shown in blue and Md_coarse is shown in pink.

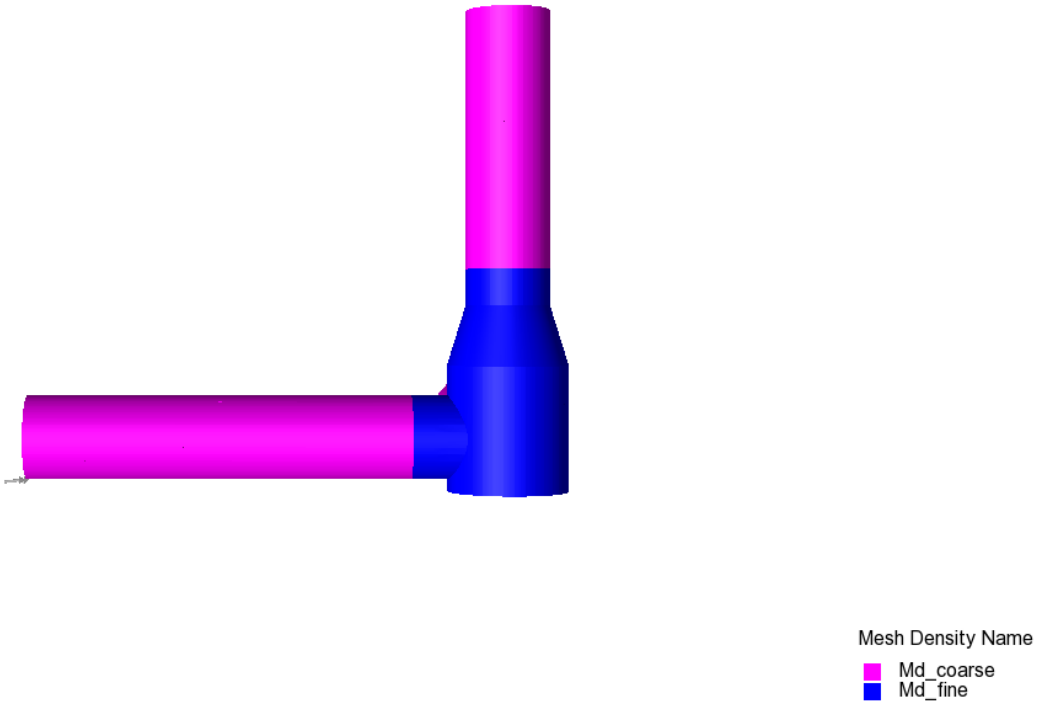

Figure 7-1 Mesh Distribution Conic Model

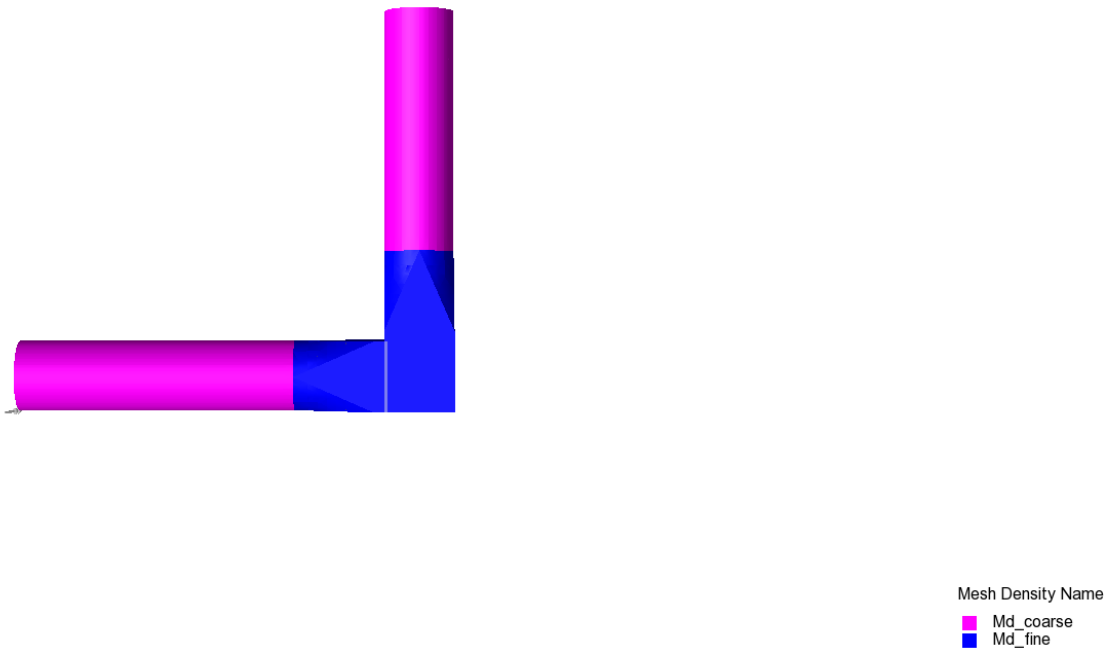

Figure 7-2 Mesh Distribution Box-Model

The mesh rules were edited

- Second order elements, using front quad mesher
- Allowing triangular elements
- Linear variation

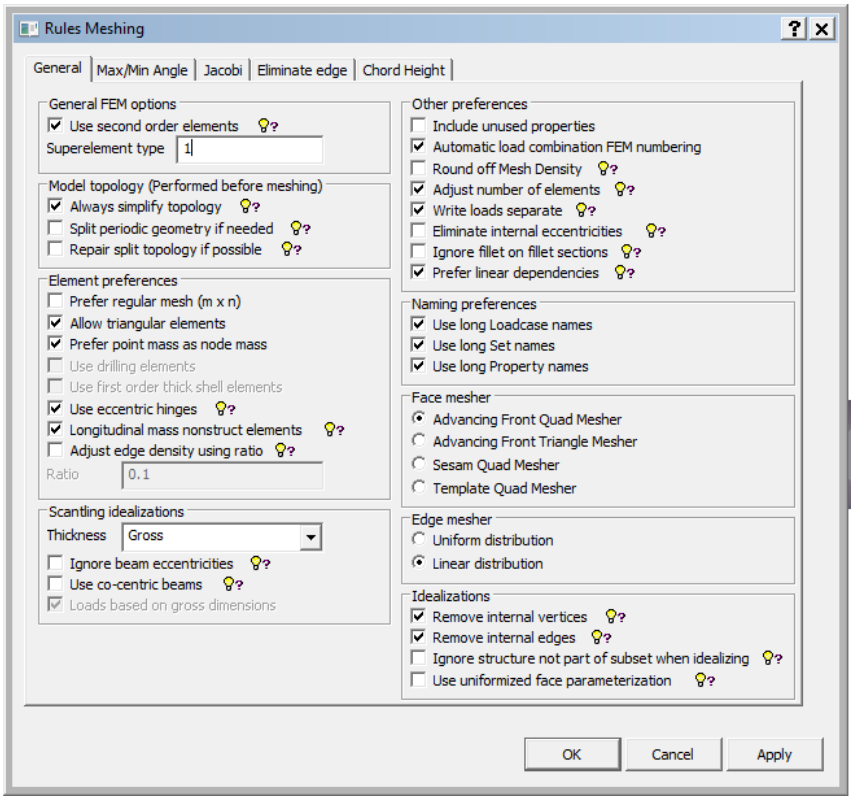

7.2 Boundary conditions and Supports

7.2.1 Supports

Support curves are added to the shell edge at the top of the column. Boundary conditions are added to these support curves.

On the free end of the pontoon a rigid link support is added. The rigid link is a connection between an independent point, called a master node and dependent nodes, called slave nodes. The slave nodes in the model inherit both the rotational and translational displacement from the master node. Displacements that are a result of analysis of a global model of the fish farm are added to the rigid link.

7.2.2 Boundary conditions

The boundary conditions are added to the supports and are given in Table 7-1 Boundary Conditions. The prescribed displacement is added to the free end of the pontoons as a load case. In the analysis these displacements are added in the load case “Displacements”. The prescribed displacements are found using a global model in GeniE. The top of the column in the models is fixed for translational displacement. The displacements added to the pontoon ends are therefore relative to the fixed top.

Table 7-1 Boundary Conditions

Boundary Conditions

Displacement/rotation	Unit	Top of Column	Free end of pontoon (Prescribed displacements)	
X	Metres	Fixed	-0.00935	-0.01116
Y	Meters	Fixed	-0.01118	-0.009342
Z	Meters	Fixed	0.006221	0.006295
Rx	Degrees	Free	-0.0007645	-0.00008119
Ry	Degrees	Free	0.00008084	0.0007608
Rz	Degrees	Free	-0.00007899	0.00007917

7.3 Loads

As mentioned in section 7.2 Boundary conditions and Supports the displacements are added to the free end of the pontoons in the load case “Displacements”. In addition to this load case a surface load is applied as its own load case, “Surface_load”. The surface load represents the constant hydrostatic pressure from the ocean. As mentioned, the bottom plate is set to be at 55 meters depth. The surface load is applied as a linear varying load, varying in z-direction. Since the bottom plate is located at 55 meters depth, the maximum hydrostatic pressure is calculated using Eq. 2-20 Hydrostatic Pressure

$$P_{gage} = \rho g h = 1025 \cdot 9.81 \cdot 55 \approx 553039\ [Pa]$$

The variation in hydrostatic pressure is calculated using Eq. 2-21 Linear Variation of Hydrostatic Pressure.

$$\frac{dP_{gage}}{dh} = -\rho g = -1025 \cdot 9.81 \approx 10056\ \left[\frac{Pa}{m}\right]$$

The load cases are combined in a load combination, called “LC3”.

Checking the surface load values

The surface load applied surface load is shown in the figures below. The maximum and minimum values correlate with the expected values, as the column has a hight of 40 meters.

Expected minimum value: $553039 - 40 \cdot 10056 = 150799[Pa]$

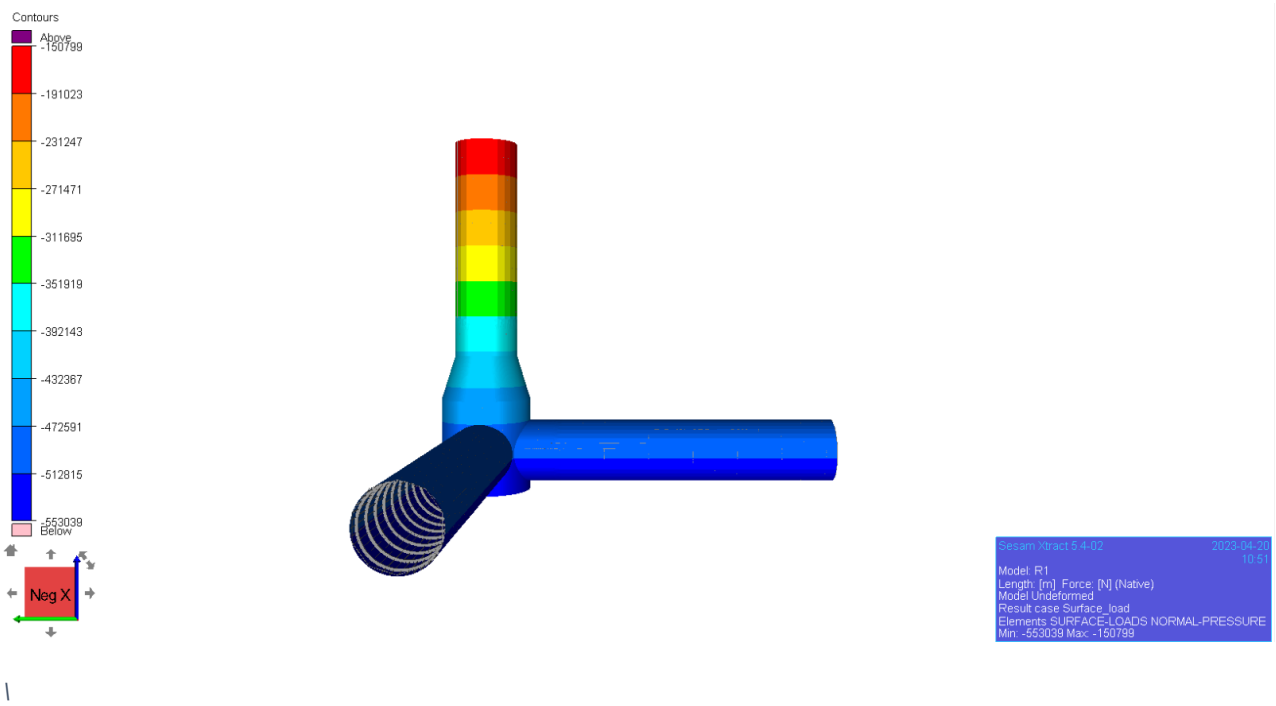

\

Figure 7-5 Hydrostatic Pressure Distribution on the conic-model

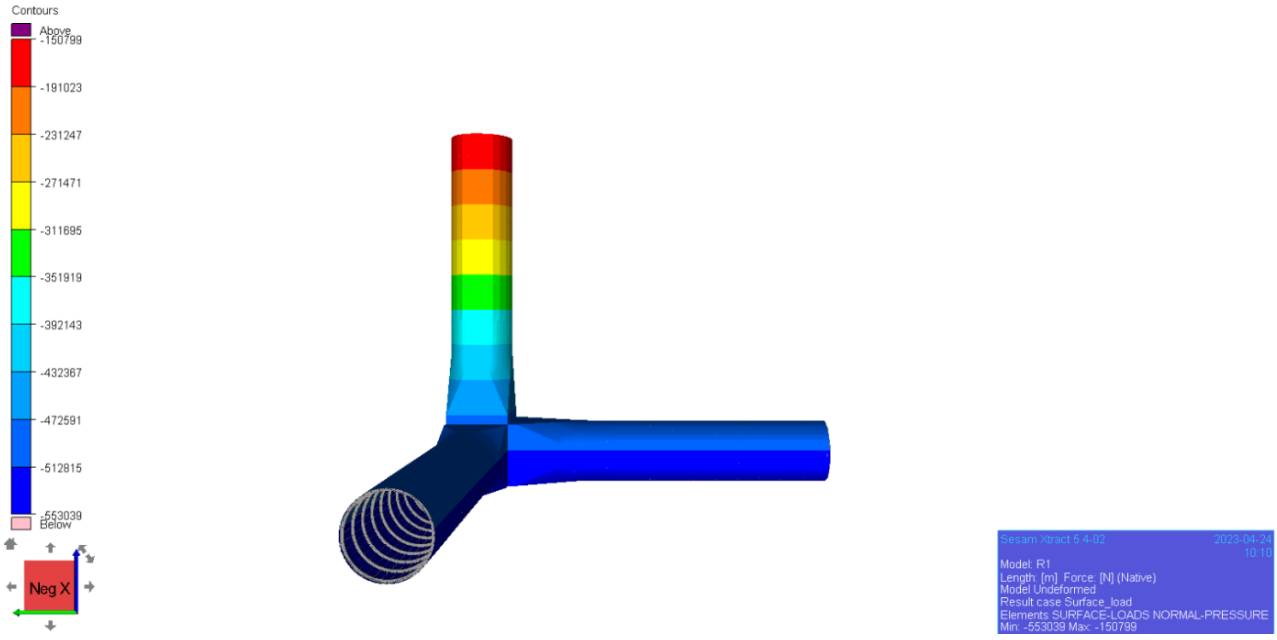

Figure 7-4 Hydrostatic Pressure Distribution on the box-model

8 RESULTS

The result from the linear static analysis is postprocessed in xtract. All results are for surfaces on the outer shell (the shell in contact with water).

The units are:

- Displacements: Meters [m]
- Von Mises stress: Pascal [Pa]

Note that the result legend is altered to visualize the local variation in stress concentration better.

8.1 The Conic Model

8.1.1 Local Displacements

The nodal displacements for all degrees of freedom caused by the hydrostatic pressure are shown in the figures below. The displacements caused by the hydrostatic pressure are of interest as they cause local deformation. The displacements added to the end of the pontoon cut boundaries are not included as they cause displacement of the entire structure (total spatial displacement also known as global displacement).

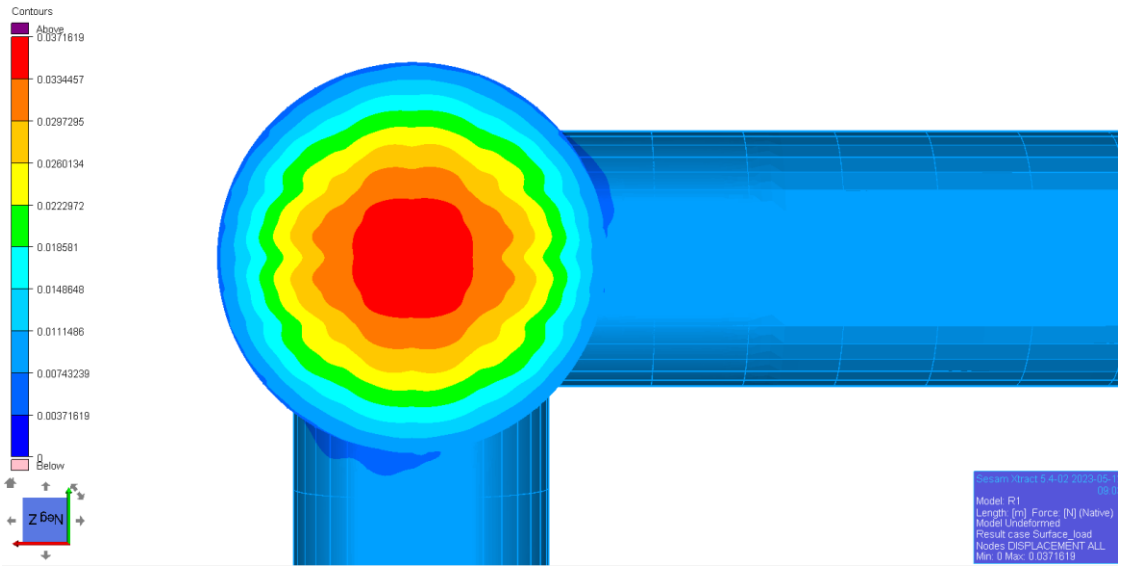

Figure 8-1 Displacements, bottom view of the conic-model

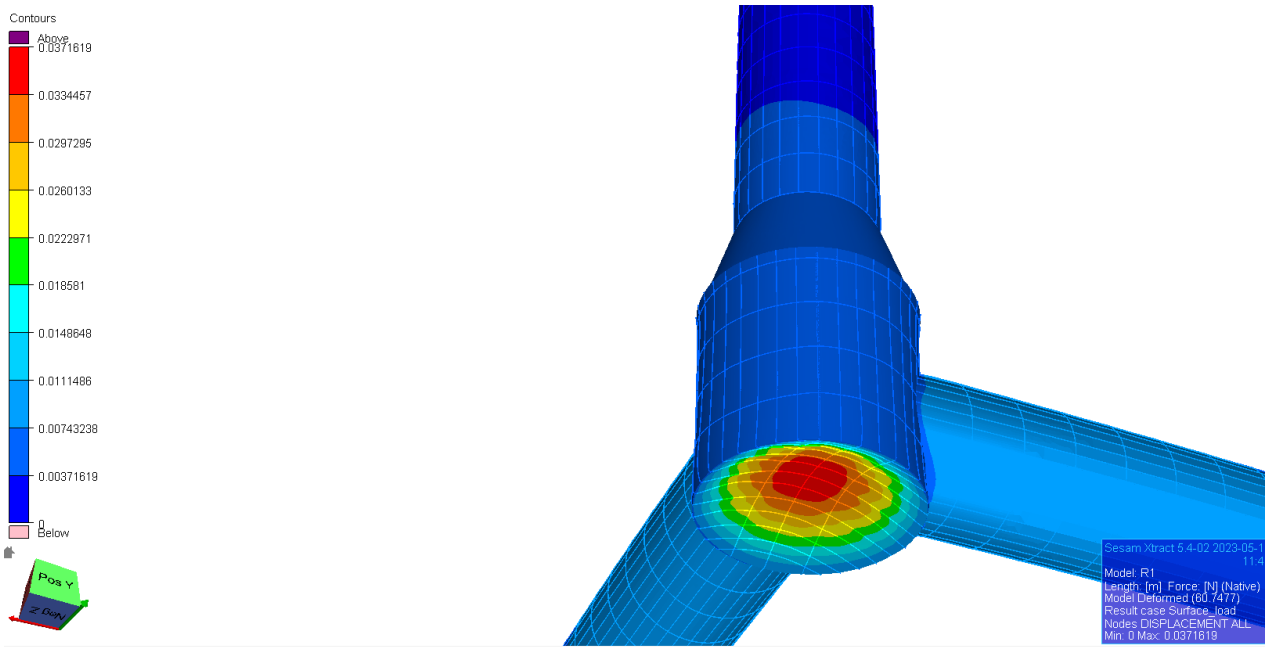

Figure 8-2 Deformation, bottom view of the conic-model

It is shown in Figure 8-1 that the maximum displacement of the conic-model is located central on the bottom plate. The maximum displacement is 3.72 cm in the z-direction (upwards) as shown in Figure 8-2, showing the deformed shape.

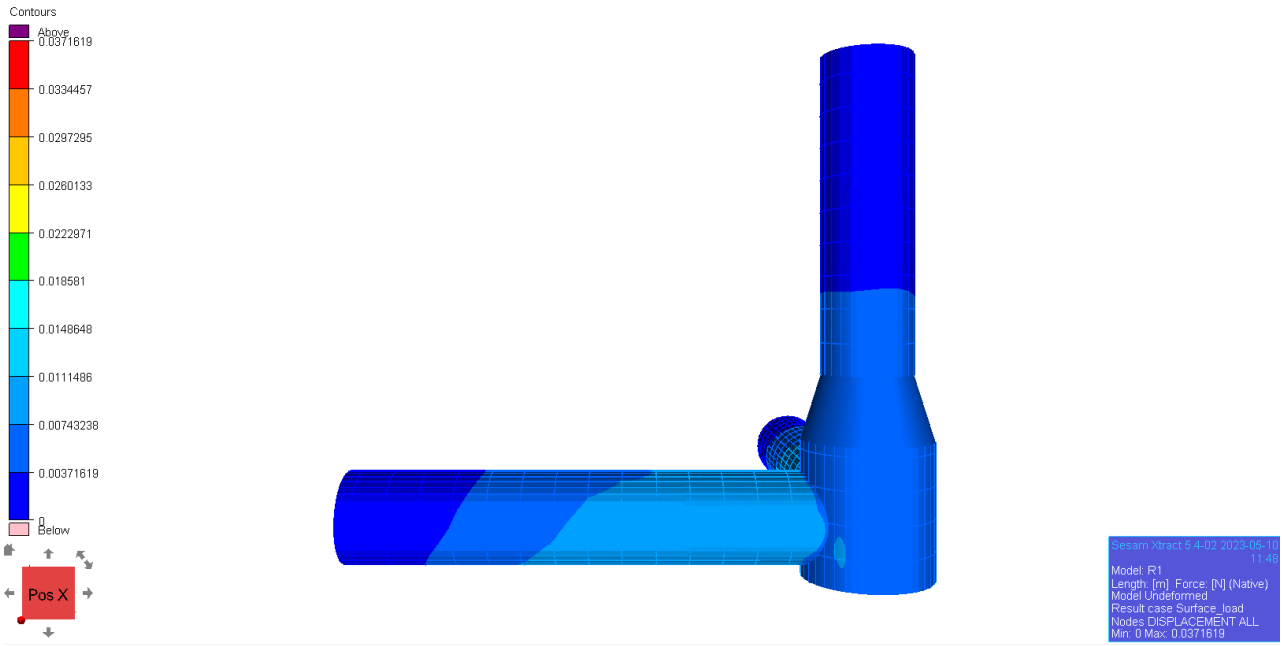

Figure 8-3 Displacements of the conic model, side view

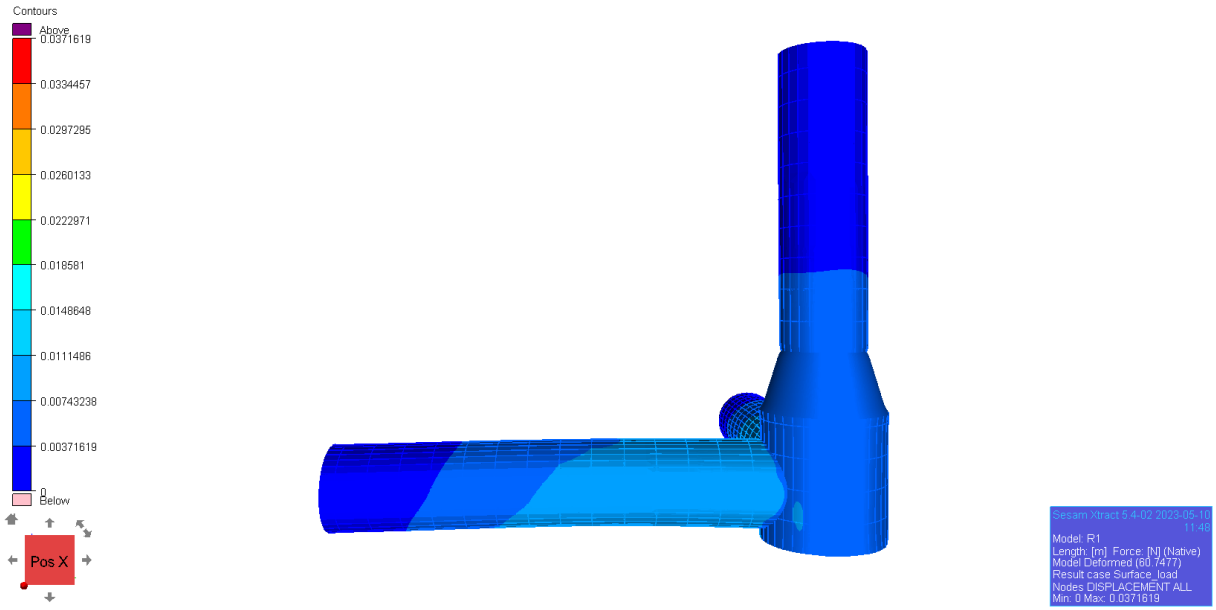

Figure 8-4 Deformation of the conic model, side view

Figure 8-3 and Figure 8-4 and shows the undeformed and the deformed shape of the conic- model from the side respectively. As shown, there are verry little deformation of the model.

8.1.2 Von Mises

The von Mises stress results from both load cases (LC3 = the hydrostatic pressure and the displacements) are shown in the figures below. The unit on the result legend is Pa.

8.1.2.1 General Von Mises

The general von Mises stress, shows the combined effect from bending stresses as well as membrane stresses (axial stresses) .

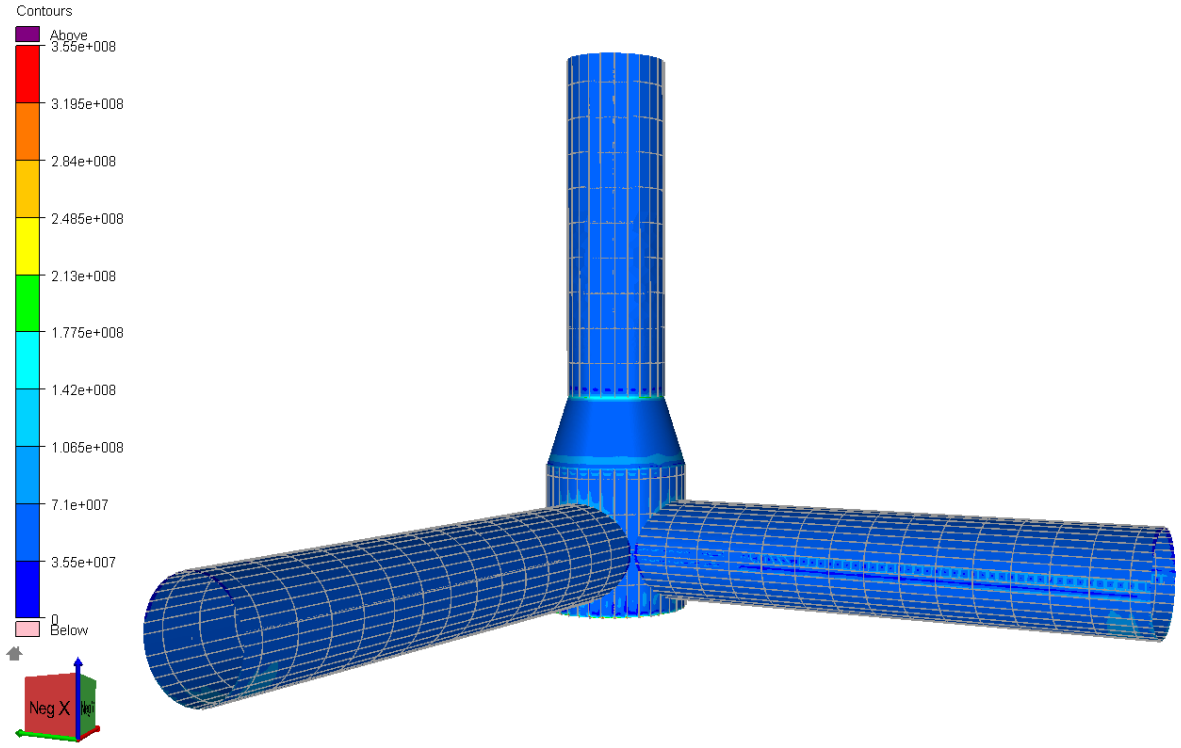

Figure 8-5 General von Mises of the conic-model. Result legend 0-355 MPa

Figure 8-5 Shows the general von Mises stress on the conic-model. It is shown that the general von Mises stress is low for all parts of the conic-model. The values are considered low as the von Mises stresses are way lower than the yield strength (355 MPa).

Note that the result legend is altered to visualize the local variation in stress better.

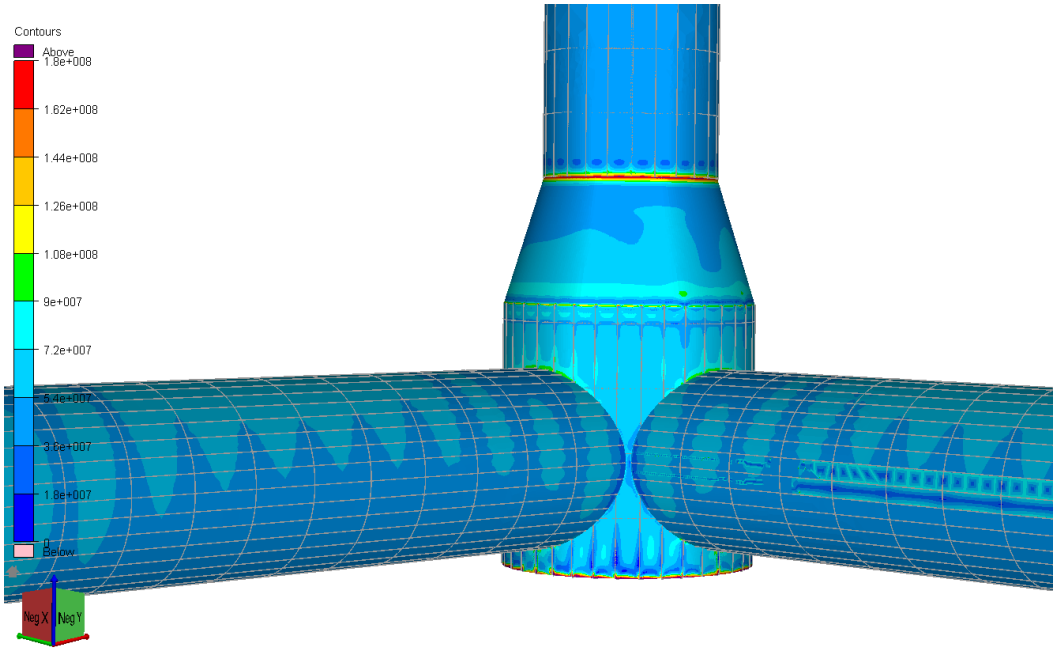

Figure 8-6 General von mises of the conic-model. Result legend 0-180 MPa

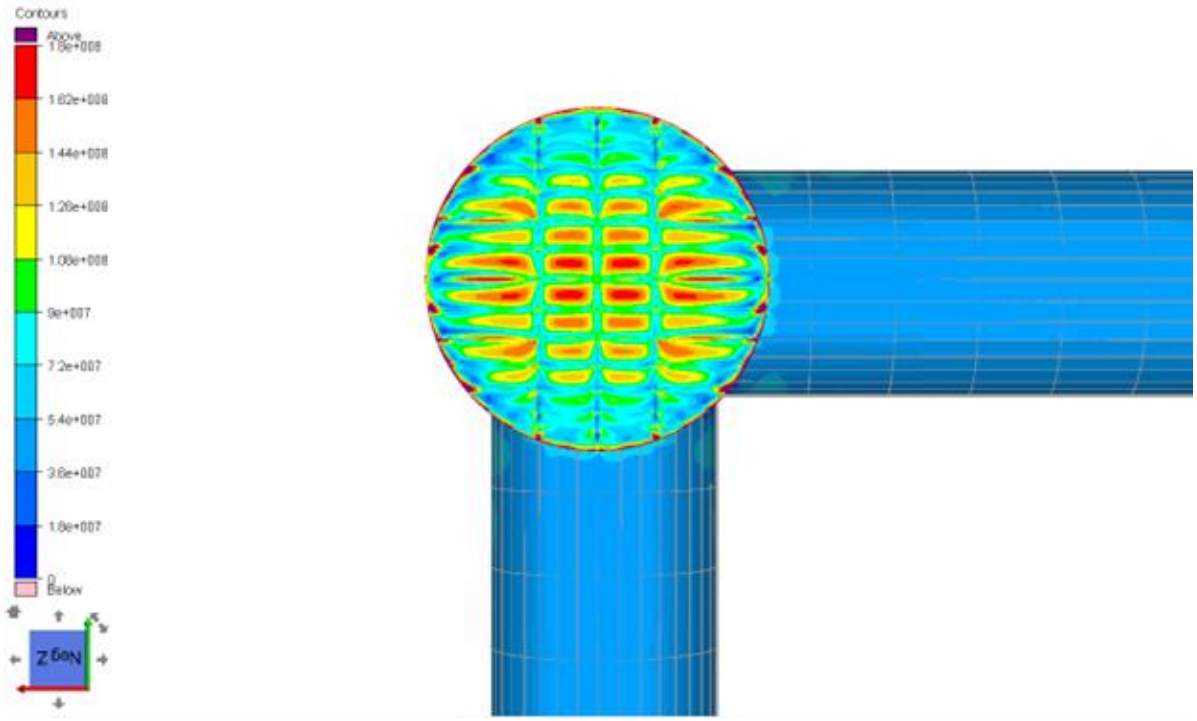

Figure 8-7 General von mises, bottom view of the conic-model. Result legend 0-180 MPa

It is shown in Figure 8-6 and Figure 8-7 that general von Mises stress occur in the transition between the conic-transition part and the upper part of the column. In addition, the highest stress level occurs at the bottom plate, between the stiffeners.

8.1.2.2 Von Mises of the Membrane

As mentioned, the von Mises stress of the membrane excludes the bending stresses. Thus, only the axial stresses are shown in the figures below.

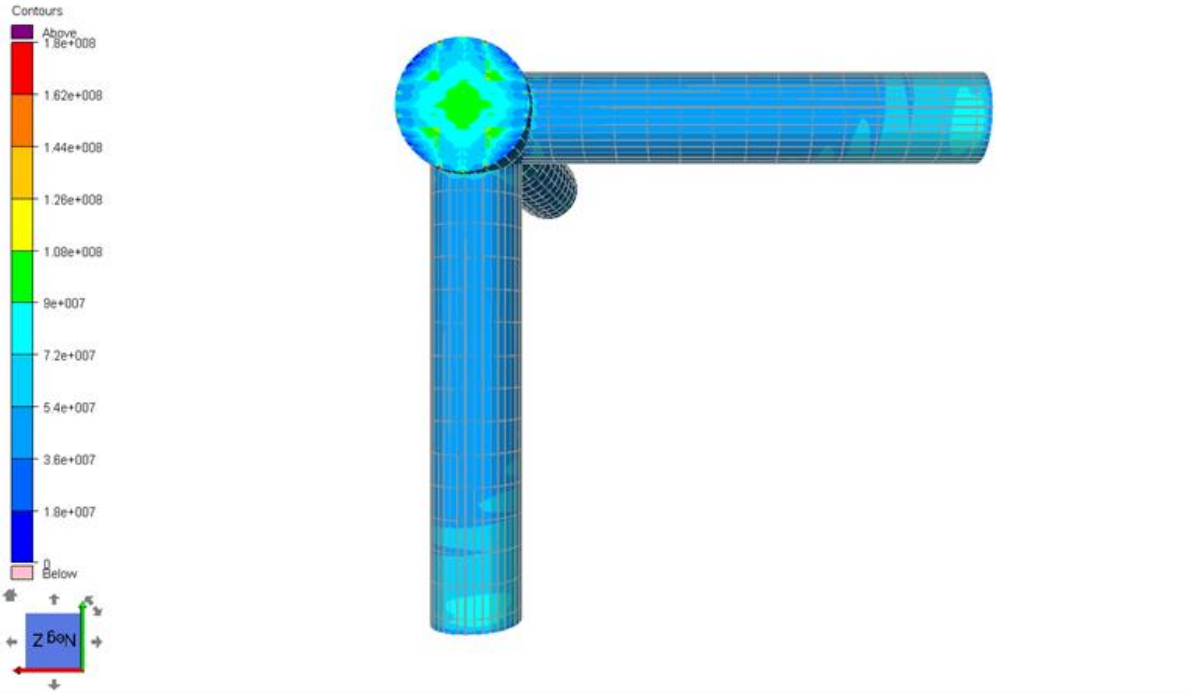

Figure 8-8 Von Mises of the membrane, bottom view of the conic-model. Result legend 0-180 MPa

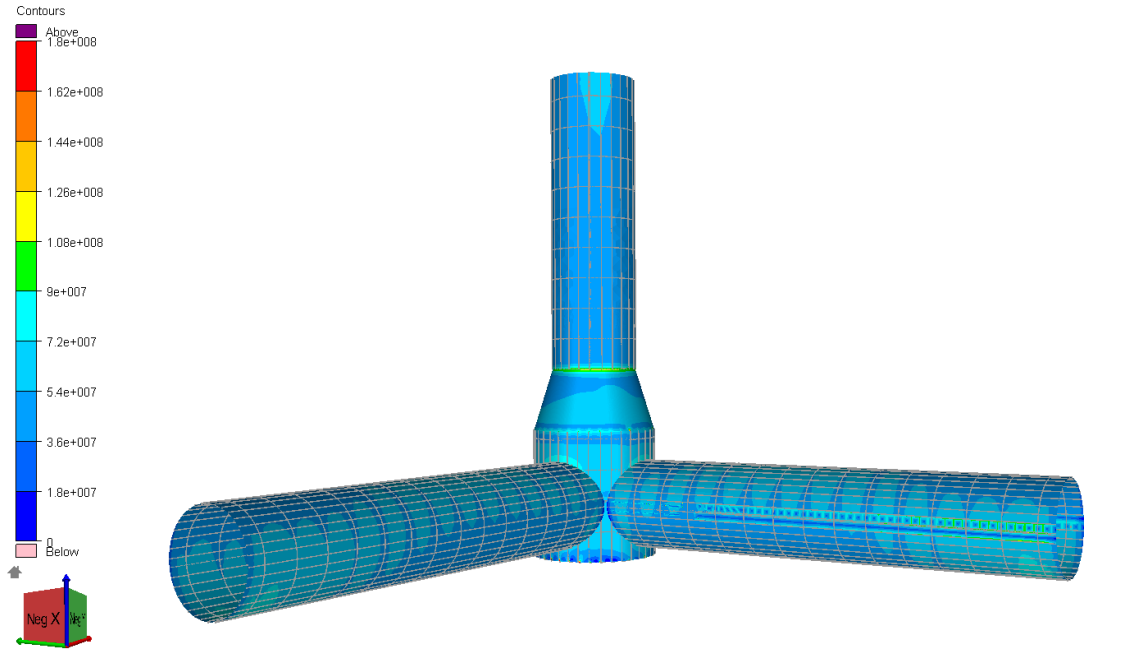

Figure 8-9 Von Mises of the membrane, conic-model. Result legend 0-180 MPa

Figure 8-8 and Figure 8-9 show that the membrane stresses are low for all parts of the conic-model.

New result legend is added to show the local variation of von Mises stress of the membrane.

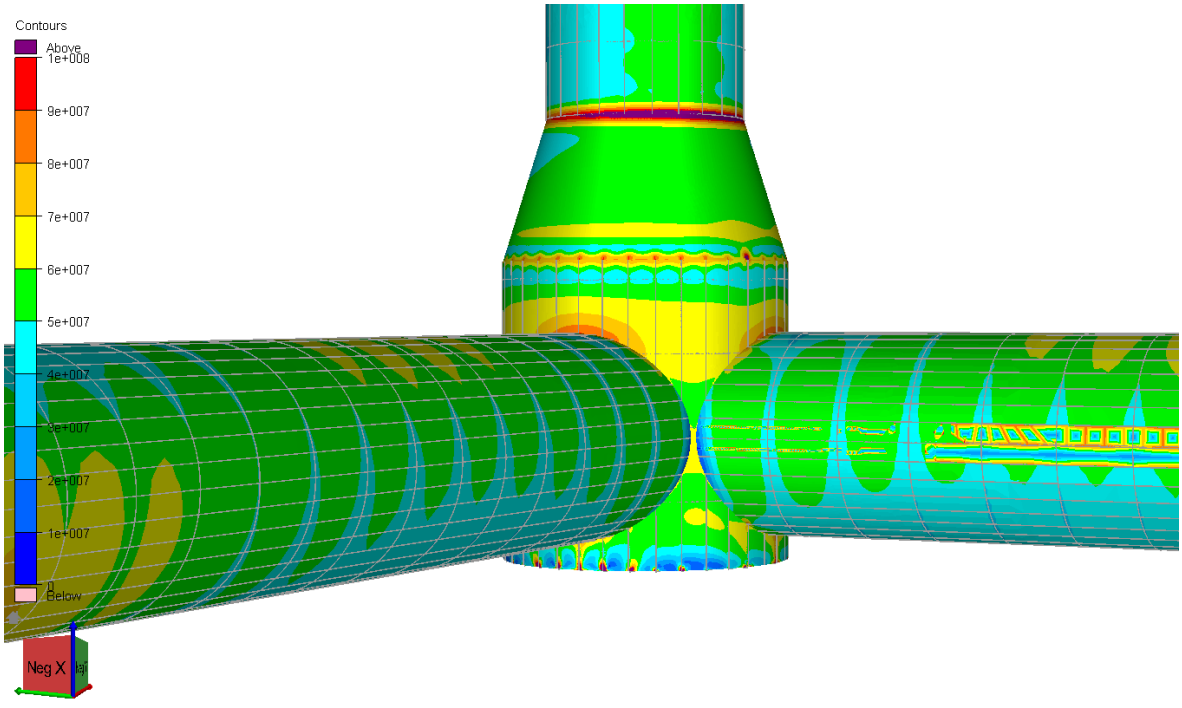

Figure 8-10 Von Mises of the membrane. Result legend 0-100 MPa

8.1.3 Material Used

The material usage of the conic-model is based on the weight of the total model. The weight is found for

- The external plating
- The internal Structure
- The sum of these

Table 8-1 Weight of the Conic-Model

Weight of the Conic-Model

Part of structure	Weight [kg]
External plating	730573
Internal structure	106624
Sum	837197

8.2 The Box Model

8.2.1 Local Displacements

The total nodal displacements caused by the hydrostatic pressure (the surface load) are shown in the figures below as they cause local deformation of the plates.

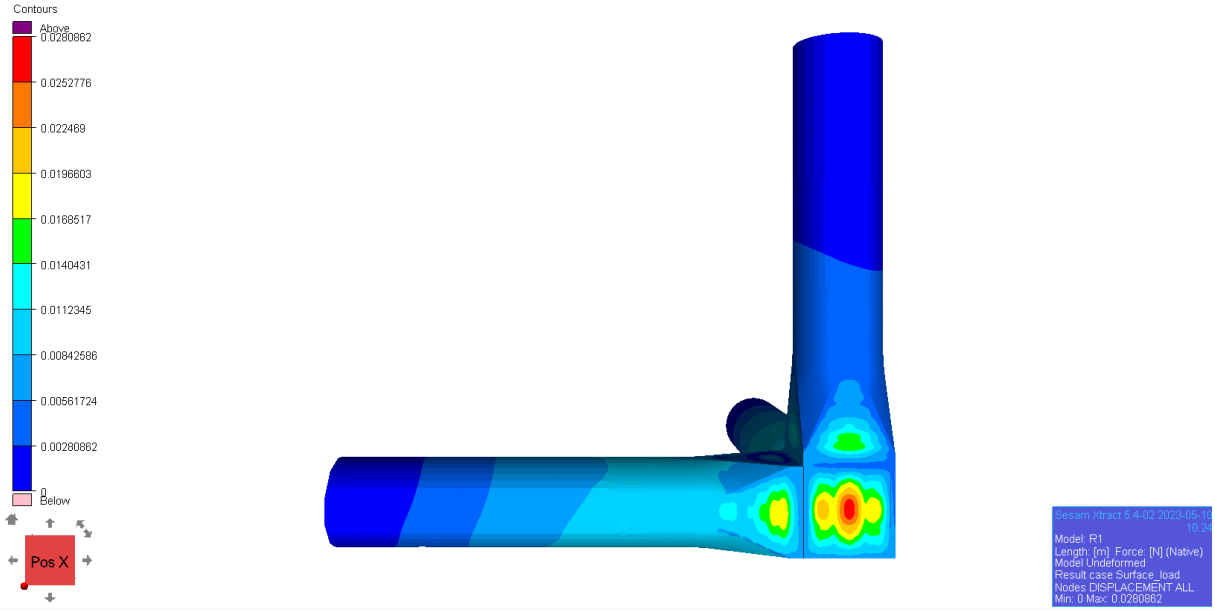

Figure 8-11 Displacement, side view of the box-model

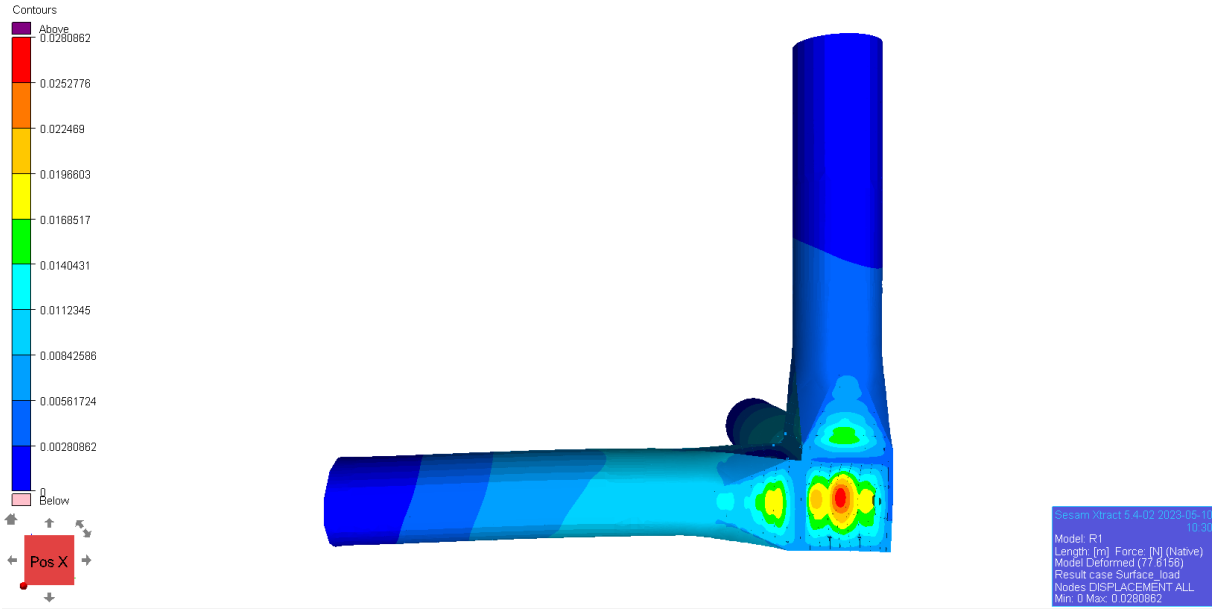

Figure 8-12 Deformed shape, side view of the box-model

The undeformed and deformed shape of the side of the box-model is shown in Figure 8-11 and Figure 8-12 respectively. It is shown that the maximum displacement caused by the hydrostatic pressure is 2.8 cm. The maximum displacement is located on both side panels of the box. The two sides are symmetric and thus have the same displacements. The figures also show that the displacement of the model in general I low.

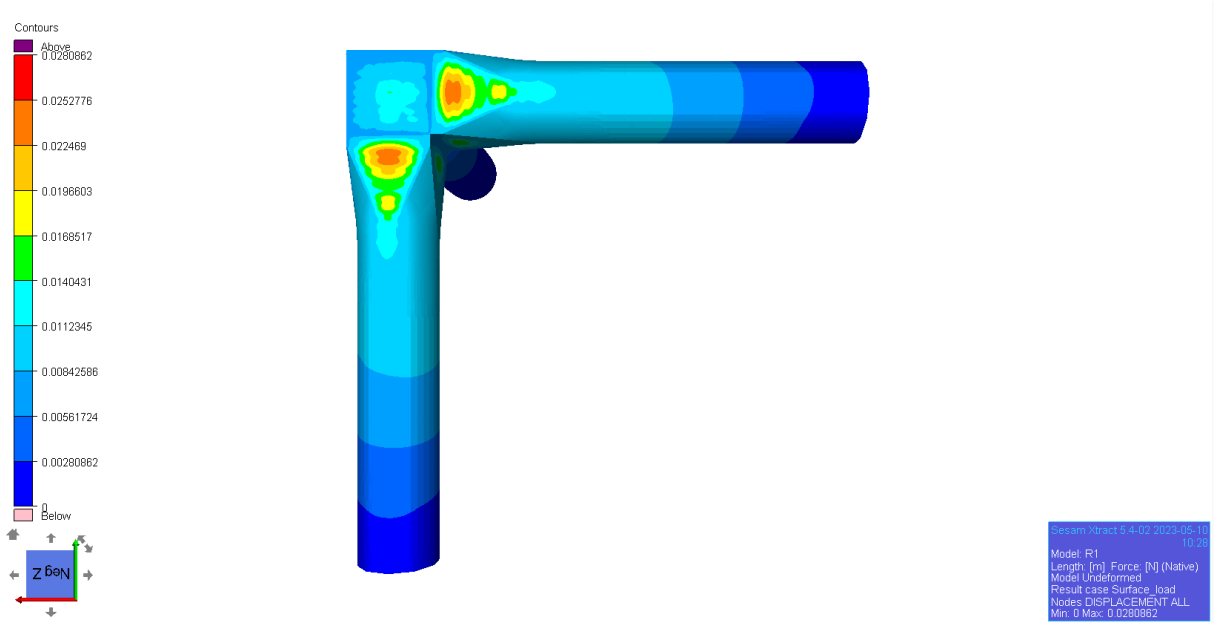

Figure 8-13 Displacements, bottom view of the box-model

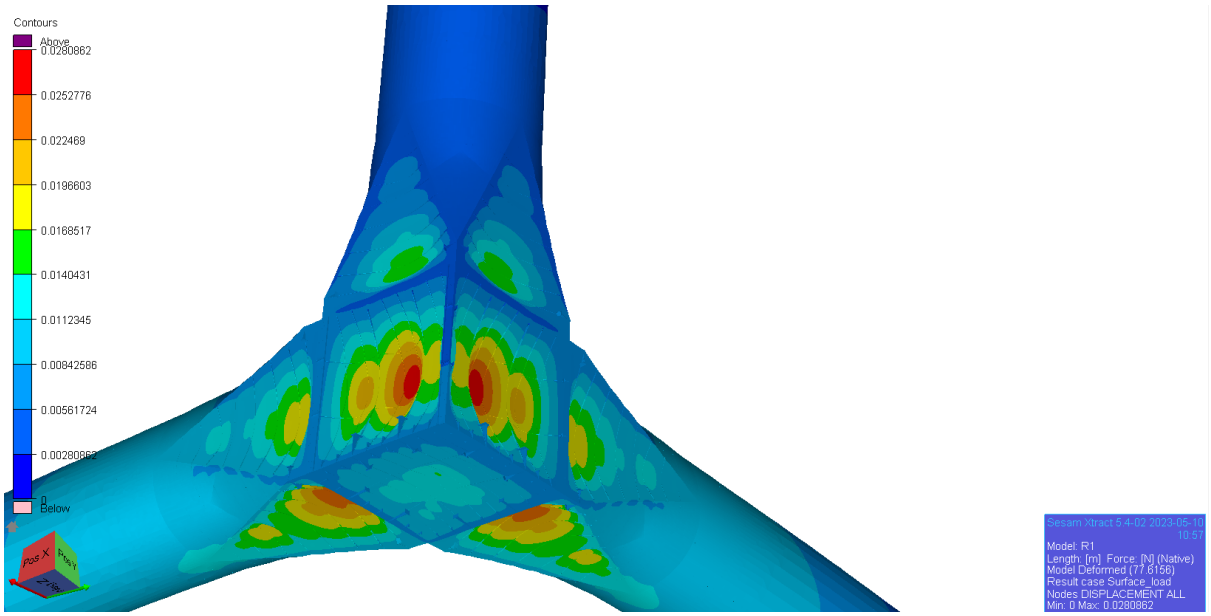

Figure 8-14 Deformed shape, view of the box-model

8.2.2 Von Mises

The von Mises stress for the load combination LC3 is given below.

8.2.2.1 General Von Mises

The general von Mises stress for the box-model is shown in the figures below:

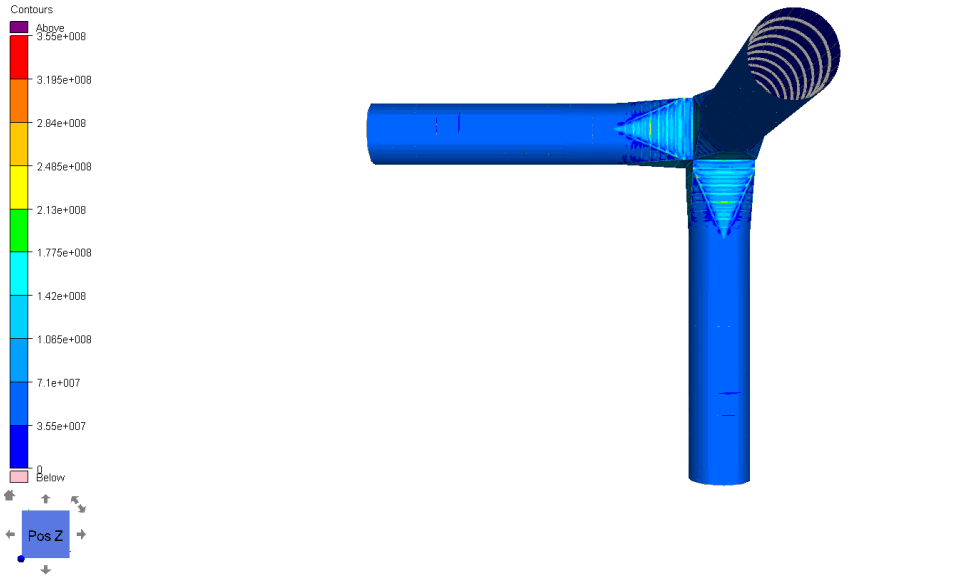

Figure 8-15 General Von Mises, top view of the box model. Result legend 0-355 MPa

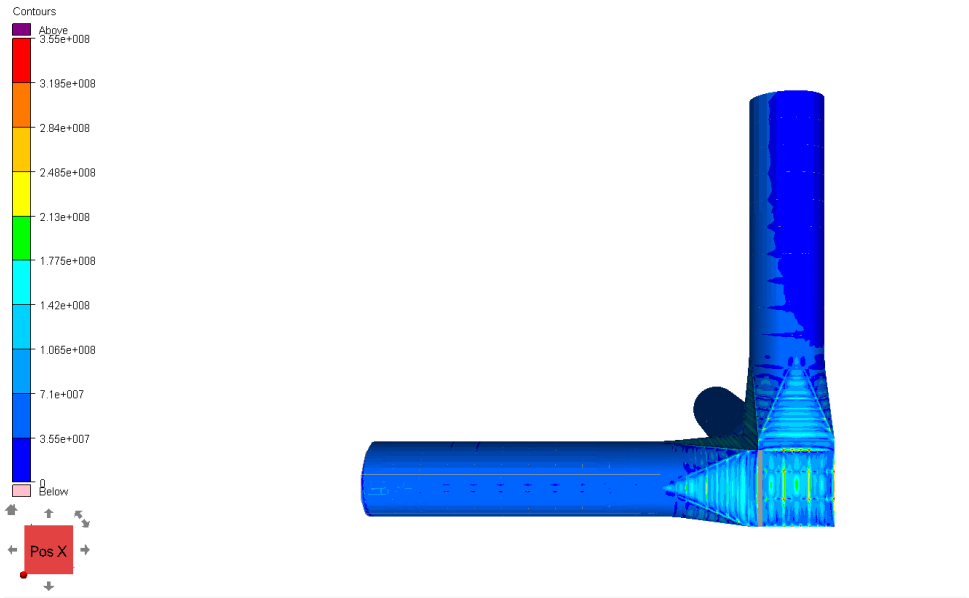

Figure 8-16 General Von Mises, side view of the box model. Result legend 0-355 MPa

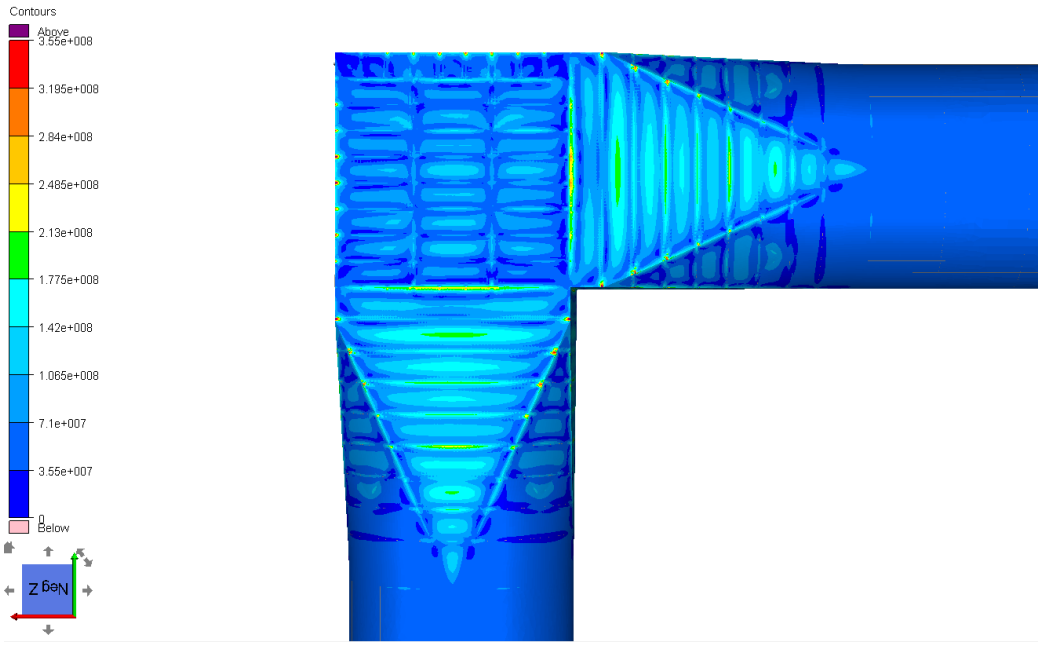

Figure 8-17 General Von Mises, bottom view of the box model. Result legend 0-355 MPa

Figure 8-15, Figure 8-16 and Figure 8-17 shows that the general von Mises stress is low for the entire box-model and less than the yield strength of steel. The box-model has general higher stress in the transition-zone between the pontoons and the column.

8.2.2.2 Von Mises of the Membrane

Note that the result legend is altered to visualize the local variation of membrane stress:

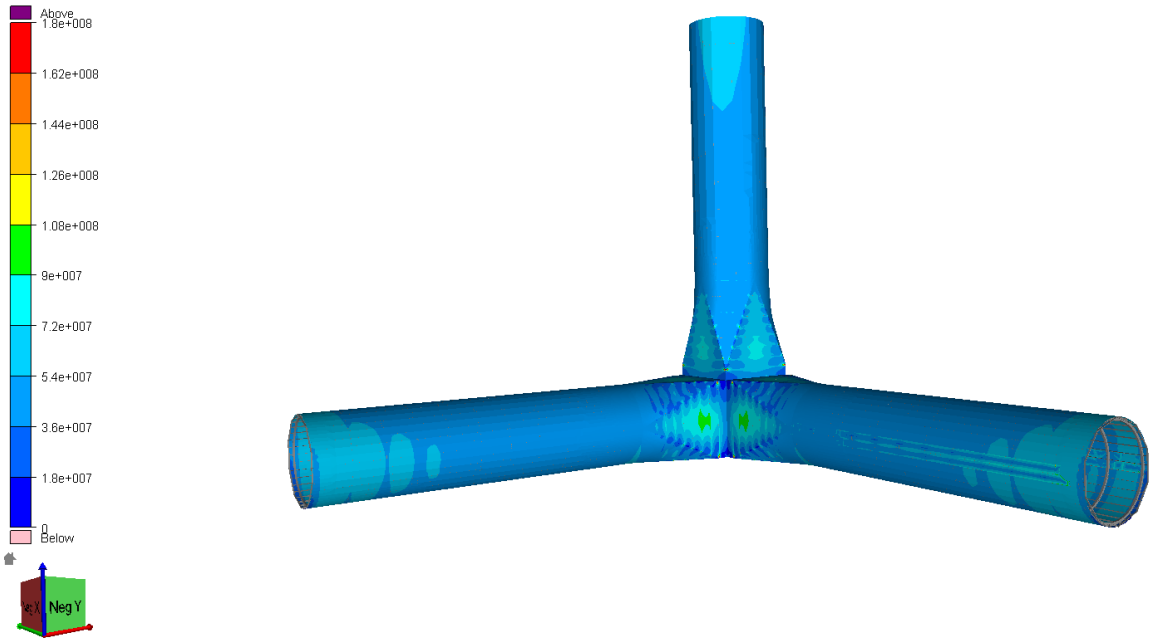

Figure 8-18 Von mises of the membrane, box-model. Result legend 0-180 MPa

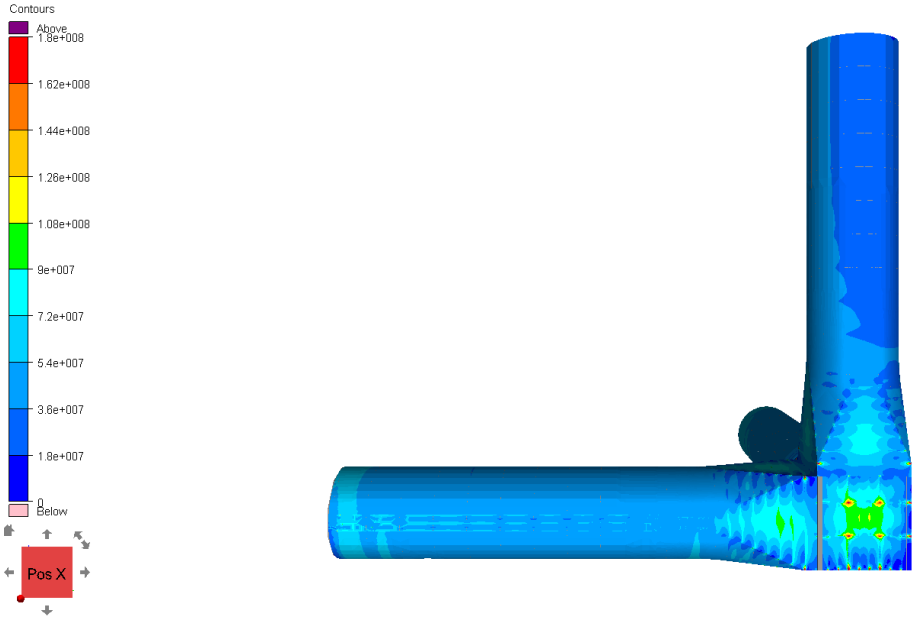

Figure 8-19 Von Mises of the membrane, side view of the box-model. Result legend 0-180 MPa

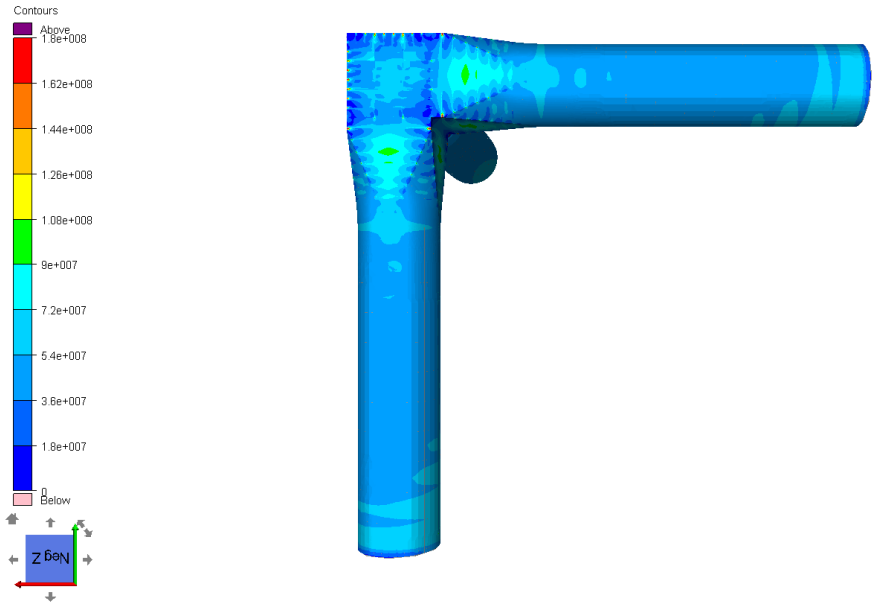

Figure 8-20 Von Mises of the membrane, bottom view of the box-model. Result legend 0-180 MPa

Figure 8-18, Figure 8-19 and Figure 8-20 shows the von Mises of the membrane for the box-model. The membrane stresses are lower than the general von Mises stresses, but the high membrane stresses are located in the same area (the transition-zone) as the high general von Mises stress.

8.2.3 Material Use

The material usage of the total box-model is based on the weight of the model.

Table 8-2 Weight of the Box-Model

Weight of the Box-Model

Part of structure	Weight of entire model[kg]
External plating	702081
Internal structure	168961
SUM	871042

9 DISCUSSION

The results for each of the models found in chapter 8

are compared and discussed in this chapter. The four criteria mentioned in 1.2 Objective lays the foundation for this discussion.

9.1 Structural Integrety

The structural integrity of the models are compared based on results from the local displacement and von Mises stress.

9.1.1 Local displacements

Checking the local displacements with the limit in DNV-OS-C101. The limit relates the span length, L, to the maximum deflection limit [4]:

$$\frac{L}{250} = max\ displacement$$

$$\frac{L}{250} = \frac{1010}{250} = 4.04\ [cm]$$

$$\frac{L}{250} = \frac{700}{250} = 2.8\ [cm]$$

The local displacements of both models are within the limits. The maximum displacement of the conic-model is 3.72 cm, this is shown in Figure 8-1. Since the maximum displacement is in the centre of the bottom plate the span length, L=10 meters (the diameter of the bottom plate). Figure 8-11 shows that the maximum displacement of the box-model is 2.8 cm. Since the displacement is located on the side panel of the box then the span length, L = 7 meters.

9.1.2 Von Mises

The von Mises stress of the membrane is of the same magnitude in both models. This can be seen in the figures in section 8.1.2.2 and 8.2.2.2. The highest membrane stress is about 100 MPa. This is lower than the yield strength of 355 MPa.

It is shown in Figure 8-5 and Figure 8-16 that the general von Mises stress which is the combined effect of membrane and bending, is higher for the box-model than for the conic-model. Especially the transition-zone between the box and the pontoons/column and the sides of the box have higher general stress, compared to the conic-model. Since the membrane stresses are about the same, the difference in general von Mises stress must be due to bending stresses. The difference in bending stresses is because of how the forces are transferred in the structure. As mentioned, stresses that are transferred as bending stresses in flat plates are transferred as membrane stresses in curved shells. The highest general von Mises stress on the side panel of the box is about 200 MPa while the highest general von Mises stress of the bottom plate of the conic-model is about 180 MPa. Despite this difference, both models have general von Mises stress well below, what is normally accepted as design criteria.

9.1.3 Hoop stress calculation

The expected hoop stress is calculated for the hydrostatic pressure is:

$$\sigma_\theta = \frac{P \cdot r}{t} = \frac{553039 \cdot 7/2}{0.035} = 55\ MPa.$$

Figure 8-9 and Figure 8-18 shows that the von Mises stress of the membrane for both models are slightly lower than the calculated hoop stress, both models have stress less than 54 MPa. The ring stiffeners may contribute this difference as they stiffen the plate.

9.2 Functionality

By comparing the functionality of the two models it shows that the curved plates of the conic-model make it less applicable for pumps and other necessary operational equipment to fit in the bottom of the column. The flat sides in the box-model are more beneficial for installation of typical modules containing operational equipment.

9.3 Constructability

The curvature of circular elements is one of the biggest challenges related to the constructability of the conic-model. Some of the issues related to the constructability of the conic-model are listed below.

- The side walls in the conic-model can be hard to roll out as the diameter is large (10.1 meter).
- It is more challenging to connect two cylindrical elements than a cylinder and a box, thus it requires more construction time (and cost).
- Transportation of circular elements can be more challenging than for elements with flat sides. The reason for this is because the circular elements will need additional supports, that are not necessary for elements with flat sides.
- The curved edged causes a lot of odd angles. Which can generate limited access for welding, inspection, and surface preparation. It will also increase the construction time as well as the time needed to design the model as all the angels need to be specified. This will increase the cost of the joint.

On the other hand, the transition-zone from the box to the pontoons/column will be the most challenging construction area of the box-model.

9.4 Material Usage

The material usage can be found by finding the weight of the structure. The material usage is compared for:

- The external plating
- The internal structure
- The sum of these

The values used in this section can be found in
Table 8-1 Weight of the Conic-Model and Table 8-2 Weight of the Box-Model in chapter 8 Results. To compare the models the conic- to- box- ratio of the masses are calculated. As some of the masses are equal for both models these masses are subtracted from the total masses, these masses can be found in the table below.

Table 9-1 Equal mass

Part of structure	Equal Mass
External plating	480251
Internal structure	44783
Sum	525033

Mass of the External Plating:

$$\frac{730573\ -480251}{702081\ -\ 480251} \cdot 100\% = 112.8$$

Mass of the internal structure:

$$\frac{106624\ -44783}{168961 - 44783} \cdot 100\% =\ 48.8\%$$

Sum

$$\frac{837197 - 525033}{871042 - 525033} \cdot 100\% = 90.2\%$$

The conic-models weight is 90.2% of the of the box-model's, thus there is a 10% difference between the models' summed mass. There is a 12.8% difference between the weight of the external plating of the models, where the conic-models has the highest weight. The biggest difference in mass-ratio is calculated for the internal structure. The mass of the internal structure of the box model is twice that of the conic-model. The reason way there is more internal structure in the box-model is because the forces are higher, as shown and discussed above.

10 FURTHER ANALYSIS

10.1 Modell Weaknesses

There are a range of weaknesses related to the models themselves. Some of these weaknesses are listed below.

- The displacements added to the end of the pontoons are the same for both models. The displacements are as mentioned from a global analysis of the fish farm. The displacements are a result from analysis of a global model using box-modelled joints. The total stiffness for a global model with conic-joint-models, would be different, and thus the displacement results would be different too. Different displacements would cause different results, than the ones found in this thesis.
- The self-weight of the joints is not included in the load cases.
- A mesh convergence study would benefit the time consumed. The mesh used in this thesis is fine, considering the dimensions of the models, and thus the results are accurate.

10.2 Optimization

Due to time shortage the joint models are not optimized. A wide range of optimizations can be done. Some examples are listed below:

- Thinner shell thickness in areas with low stress concentrations, such as the ends of the pontoons and top part of the column. This can improve the material usage. However, this can also decrease the structural integrity of the model and thus, new analysis must be run.
- Longitudinal stiffeners in the transition zone of the box, can replace the need for two different ring stiffener sections, T650x200x15x25 and T250x150x10x15
- Stiffeners in the conic transition.

10.3 Fatigue in Offshore Structures

The environmental loads, in particular the wave loads are the dominating contributor to fatigue damage in offshore structures [13]. As mentioned in section 3.6 Simplified Fatigue Calculation structural details that have high principal stress concentrations are at risk of fatigue failure. To visualize such structural parts, results from the displacement load case are presented in this section. The effect of the hydrostatic pressure is not considered, as fatigue is a concern related to time varying load. The hydrostatic pressure in this thesis is considered constant, and thus the hydrostatic pressure will have no effect on the fatigue failure of the joints. In reality, the hydrostatic pressure is non-constant and will have an additional dynamic contribution to the total pressure and thus, it will reduce the fatigue life.

The principal stresses for both models are shown in the figures below.

10.3.1 The Conic-Model

Principal stress P1

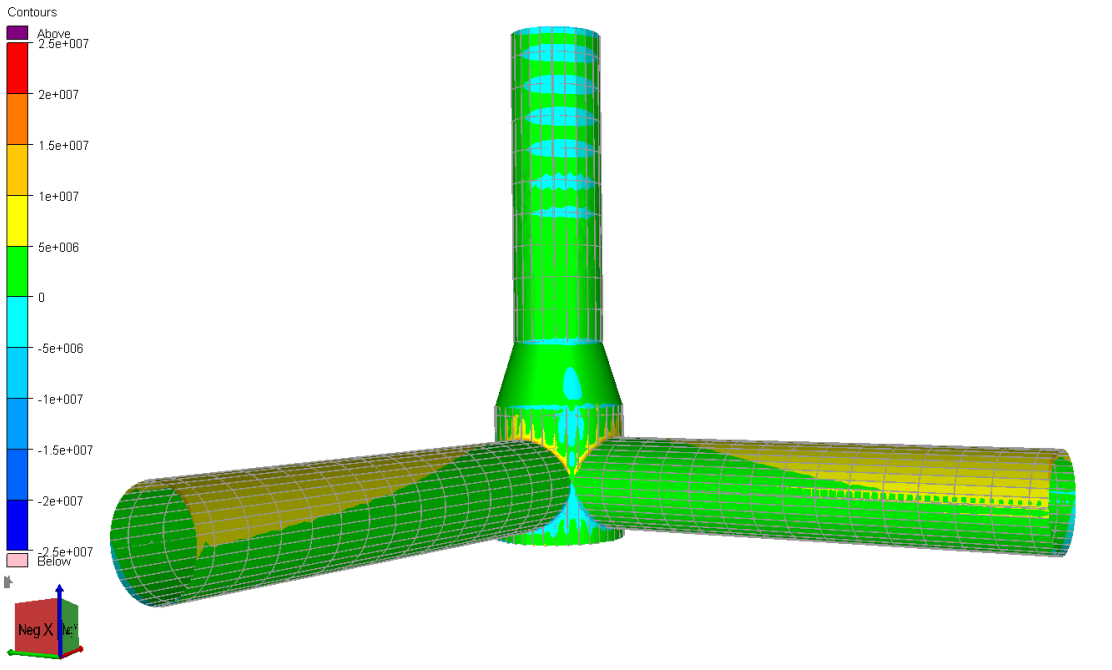

Figure 10-1 Principal stress, P1 for the conic-model

Figure 10-1 shows that the principal stress P1 is low for the entire conic-model.

To better visualise the local differences in stress the result legend is altered.

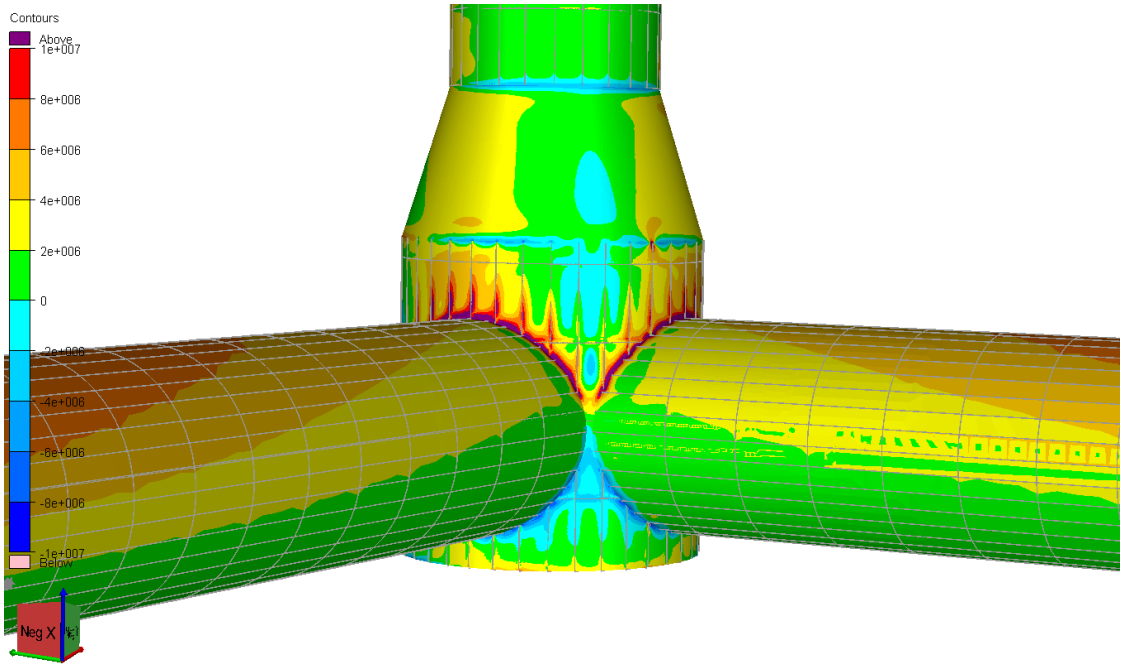

Figure 10-2 Principal stress, P1 lower result legend for the conic-model

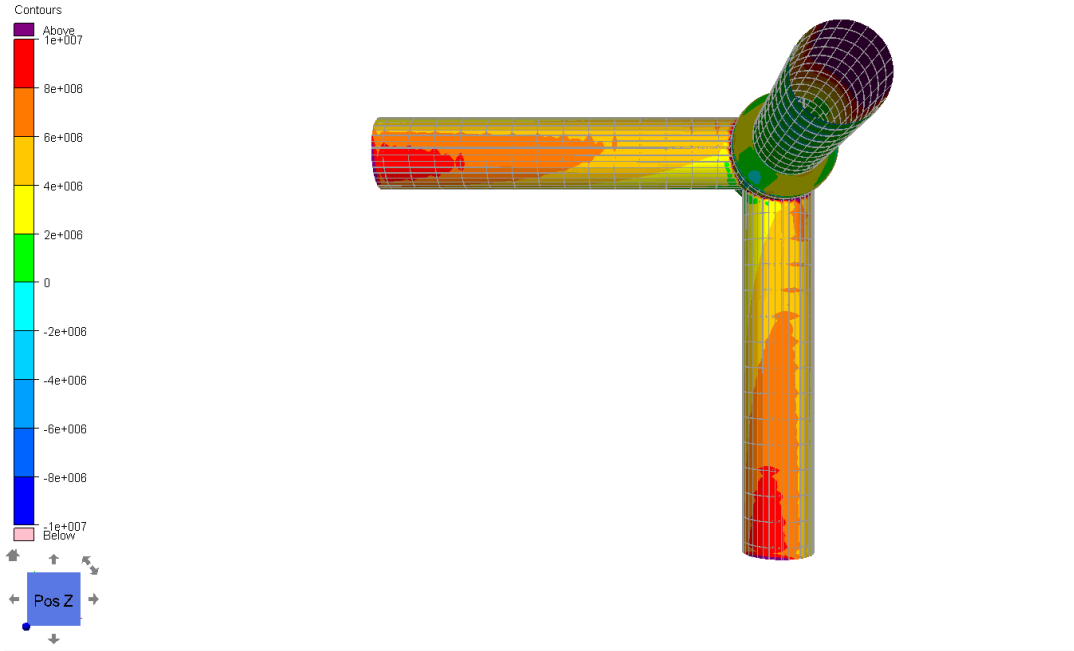

Figure 10-3 Principal stress, P1 lower result legen for the conic-model, top view

Principal stress P2

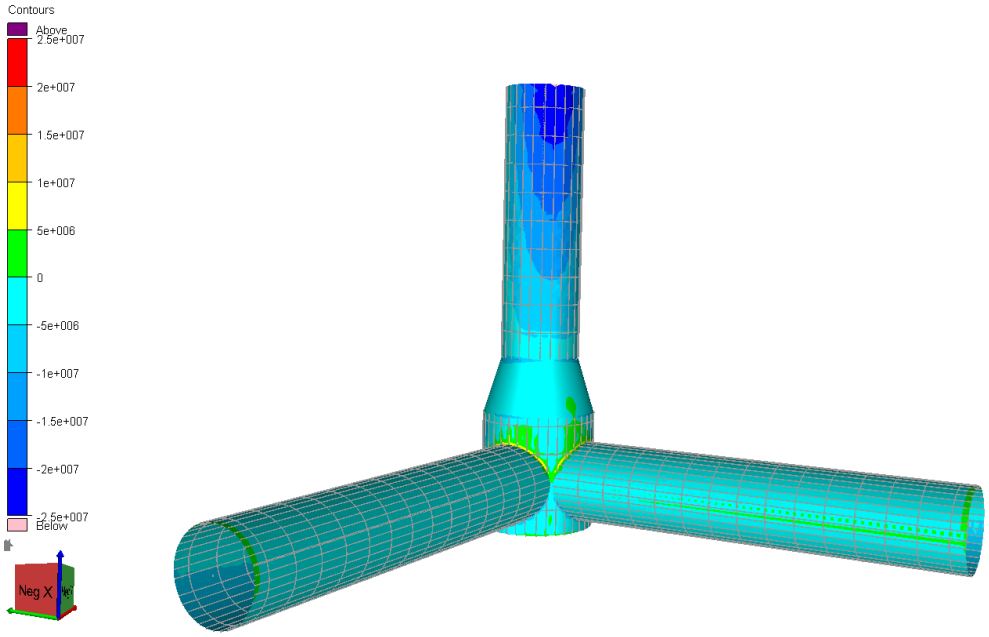

Figure 10-4 Principal stress, P2 for the conic-model

Figure 10-4 shows that the principal stress P2 also is low for the entire conic- model.

To better visualise the local differences in stress the result legend is altered.

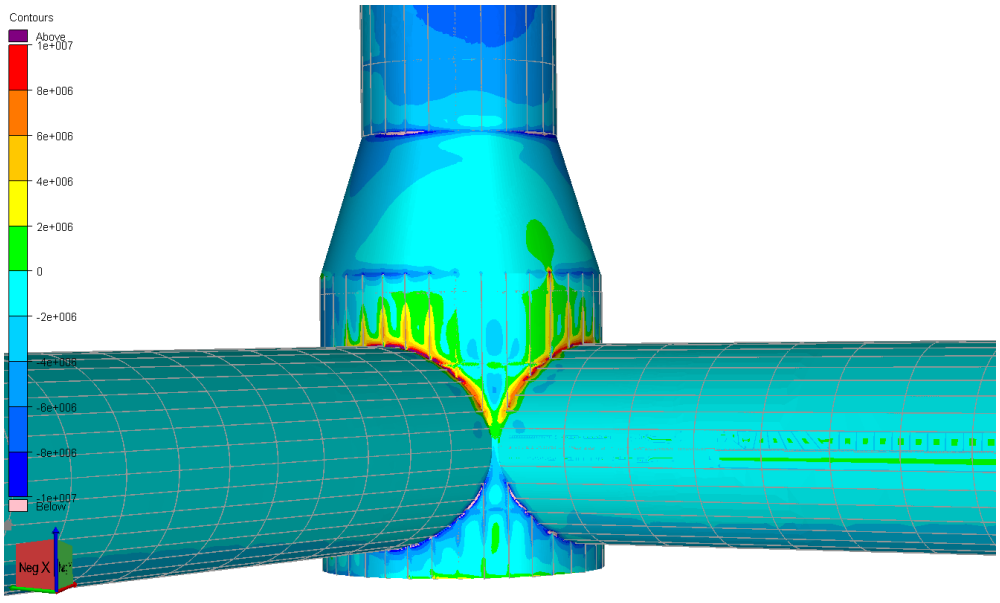

Figure 10-5 Principal stress, P2 for the Conic-model for lower result legend

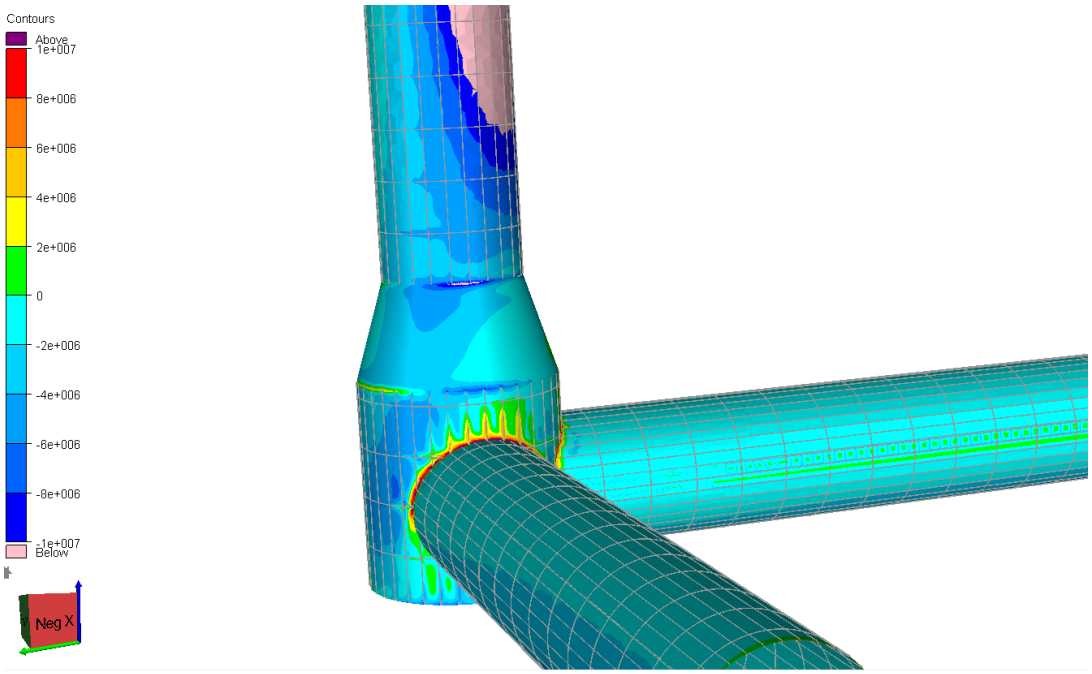

Figure 10-6 Principal stress, P2 for the conic-model

It is shown in figure 10-1 to 10-6 that the highest principal stress concentrations occur in the transition between the pontoons and the column (P1 stress and P2 stress) as well as the transition between the column and the conic-transition part (P2 stress). Thus, these areas are at risk for fatigue failure.

10.3.2 The Box-Model

The results for the principal stress P1 for the box-model caused by the displacement load is shown in the figures below:

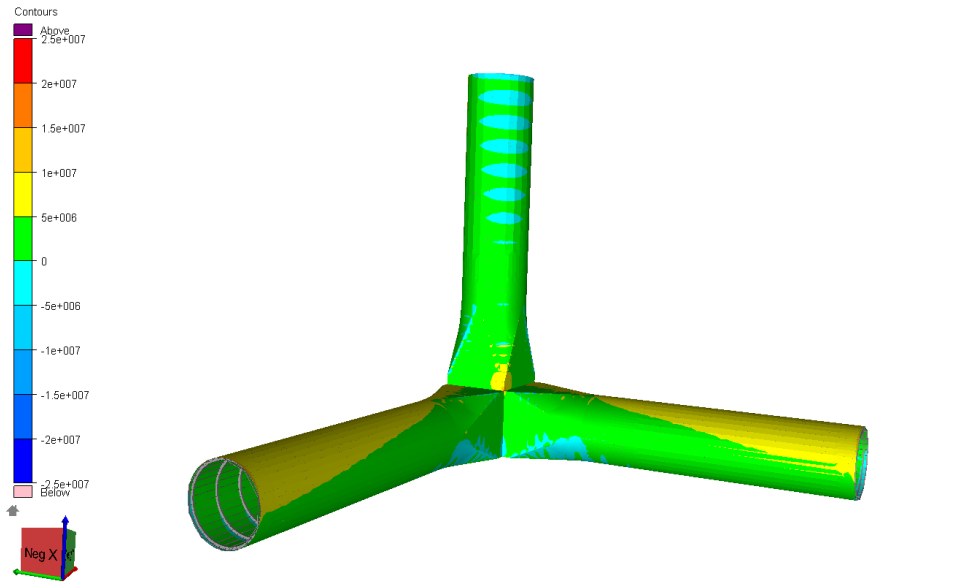

Figure 10-7 Principal stress, P1 of the box-model

Figure 10-7 Shows that the principal stress, P1 is low for the entire box-model. Figure 10-7 Principal stress, P1 of the box-model

To better visualize the local variation in stress concentrations the result legend is altered.

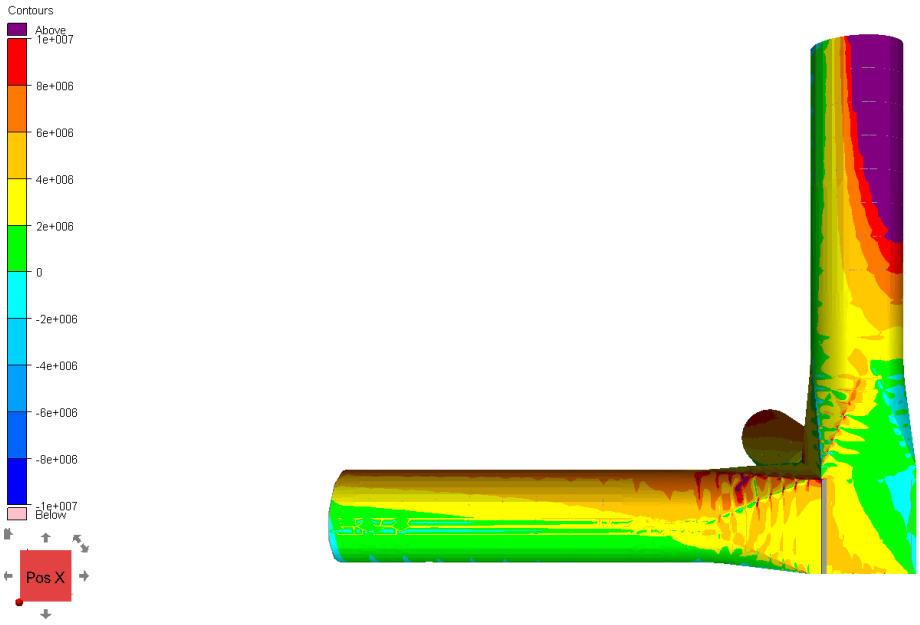

Figure 10-8 Principal stress, P1 lower result legend, side view of the box-model.

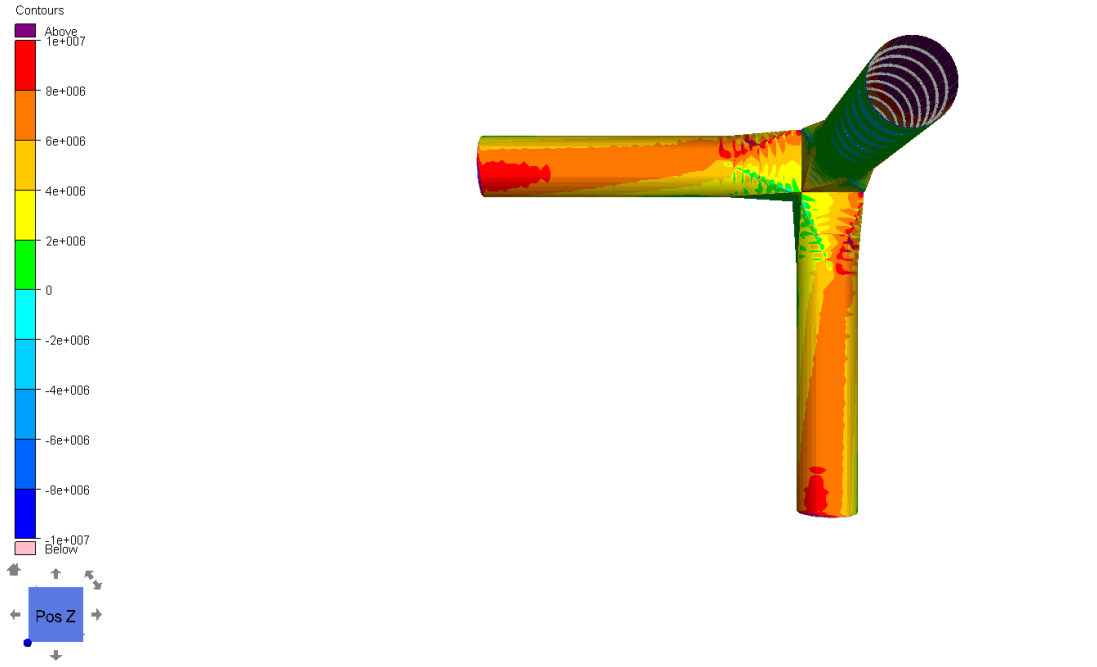

Figure 10-9 Principal stress, P1 lower result legion, top view of the box-model.

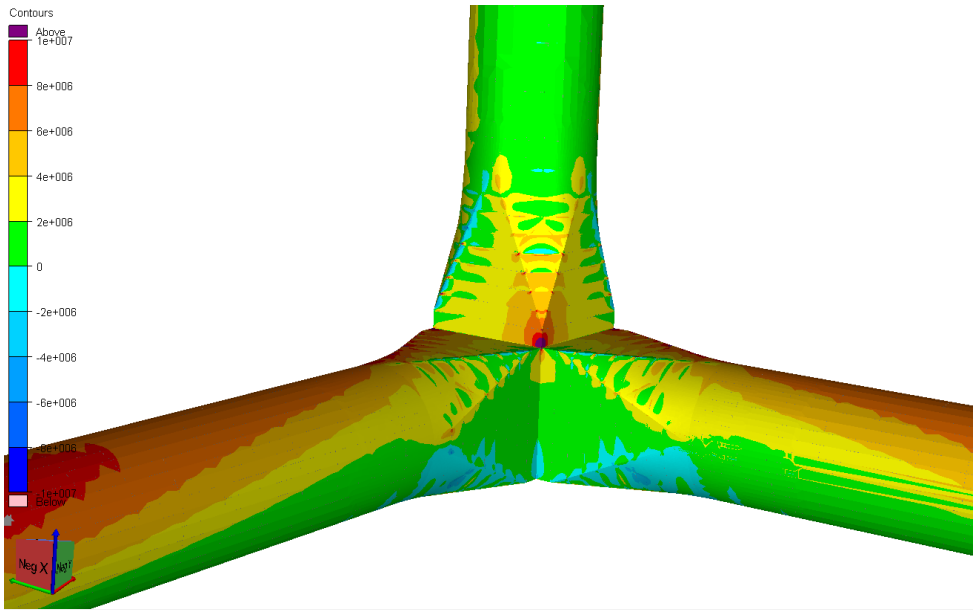

Figure 10-10 Principal stress, P1 for the box-model

The results for principal stress P2 on the box-model is shown below. Note that the result legend is altered, to show the entire model.

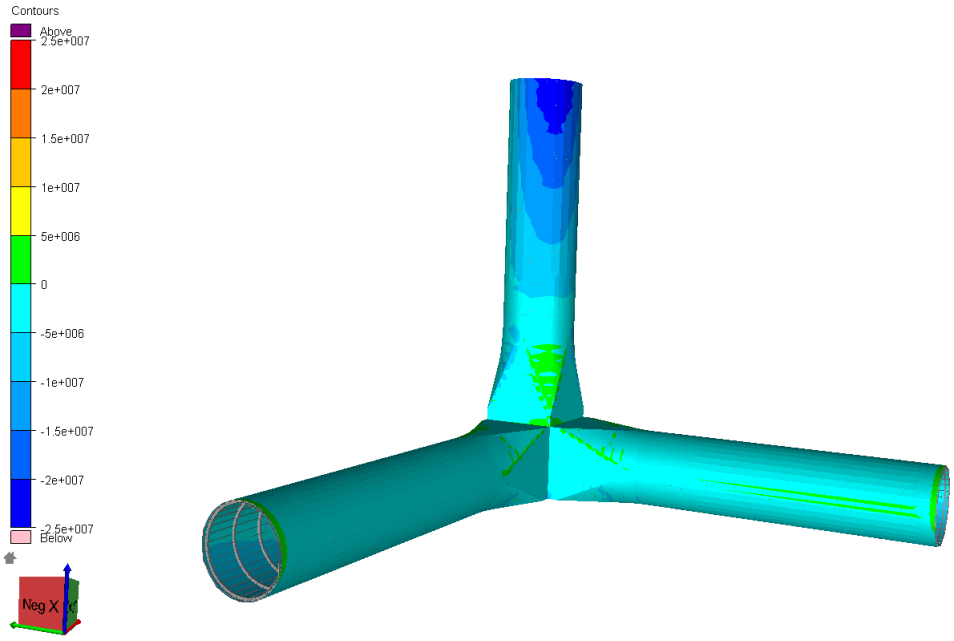

Figure 10-11 Principal stress, P2 for the box-model

To better visualize the local variation of stress concentrations the result legend lowered to ± 10 MPa.

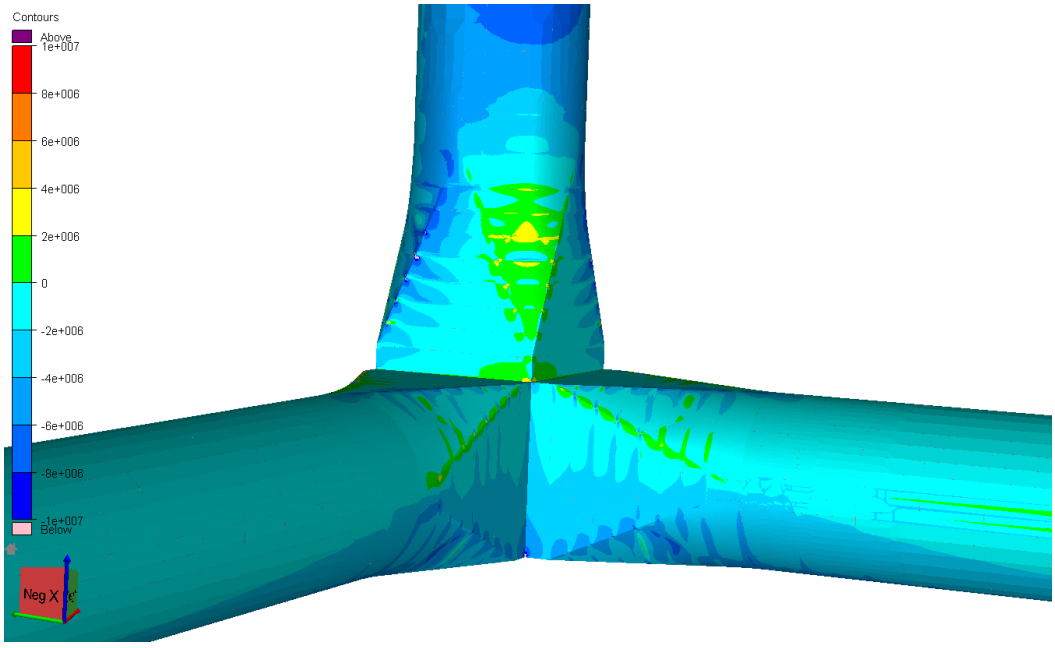

Figure 10-12 Principal stress, P2 lower result legend of the box-model.

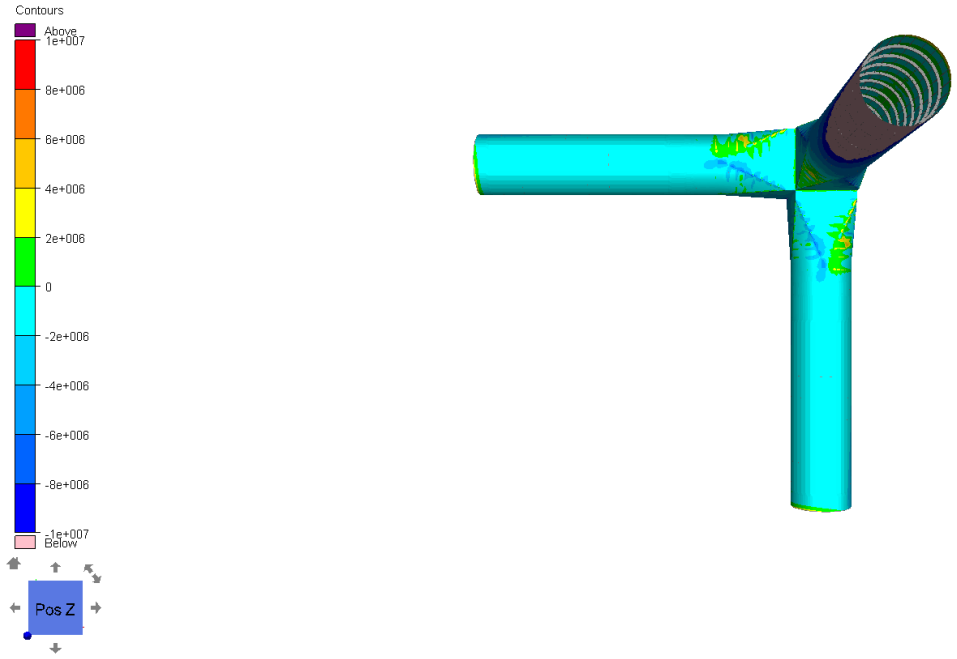

Figure 10-13 Principal stress, displacement load, top view of the box-model

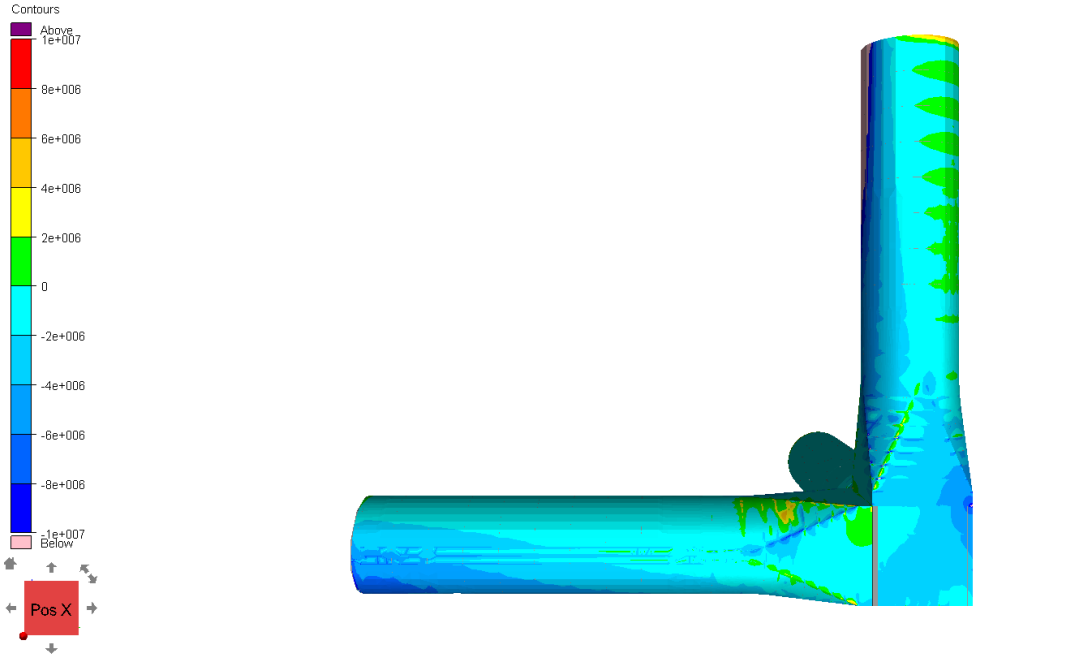

Figure 10-14 Principal stress, P2 lower result legend, side view of the box-model.

The general principal stresses of both models are at the same level. However, the box-model does not have such high stresses caused by the displacement load as the conic-model. This implies that the box-section has better fatigue capabilities than the conic-model.

11 CONCLUSION

Both models fulfil the structural integrity requirements, even though the box-model have higher stresses than the conic-model. Three load cases are analysed, a hydrostatic pressure, a displacement load and a combination of those. The displacement load is a result from analysis of a global model of the fish farm. The stress results shows that the stresses from all load cases are low, especially the stresses caused by the displacement load (ref. section 10.3 Fatigue in Offshore Structures). In addition, the displacements are within the limits according to applicable standards.

The calculated hoop stress is higher than the results shown in the analysis. This is most likely due to the internal ring stiffeners.

When comparing the weight of the models it shows that the conic-model has about 10% lower summed weight. The biggest difference in weight between the models is the weight of the internal structure. The conic-model's weight of the internal structure is about 50% of the box-model. This difference does not have any significant impact on the functionality and constructability of the models. Thus, when comparing the material usage, the total mass will be the dominating contributor to the decision, as it is related to the cost of the model.

The functionality is evaluated to be better for the box-model as it does not have curved walls in the bottom part of the cylinder. The curved edges also cause a range of constructability issues related to the transportation, odd angles, and connections between two cylinders. The constructability issues will increase the cost of the model.

To draw a conclusion, an overall evaluation is performed, and the box-model prevail over the conic-model and is therefore recommended due to the constructability and functionality issues related to the conic-model. These issues dominate over the fact that the box-model requires 10% more steel.

12 REFERENCES

[1] Regjeringen, “Norsk havbruksnæring,” *Regjeringen,* 11 10 2021.

[2] Regjeringen, «The Government’s commitment to the ocean and ocean industries - Blue Ocean, Green Future».*Regjeringen.*

[3] United Nations, “The Sustainable Development Goals Report,” United Nations, 2022.

[4] DNV, DNV-OS-C101, Design of offshore steel structures, general (LRFD method), DNV, 2011.

[5] V. Adams and A. Askenazi, Building Better products with Finite Element Analysis, Santa Fe: OnWord Press, 1999.

[6] DNV , Sesam User manual SESTRA Finite Element solver, DNV, 2021.

[7] R. Fenner, Engineering Elasticity, John Wiley & Son, 1986.

[8] R. Hibbeler, Mechanics og Materials, Pearson , 2018.

[9] Y. A. Çengel, J. M. Cimbala og R. H. Turner, Fundamentals of thermal-fluid sciences, New York, N.Y: McGraw-Hill Education, 2021.

[10] DNV, DNV-RP-C103, Column Stabilised Units, DNV, 2021.

[11] DNV, DNVGL-CG_0130, Wave Loads, DNV, 2021.

[12] A. Almar-Næss, Fatigue Handbook, Trondheim: Tapir, 1985.

[13] DNV, DNV-RP-C203, FATIGUE DESIGN OF OFFSHORE STRUCTURES, DNV, 2005.

[14] A. Fiskvatn, Elementmetoden, Trondheim: Tapir, 1984.

[15] D. Pavlou, Essentials of the finite element method : for mechanical and structural engineers, London: Academic Press, 2015.

[16] R. D. Cook, D. S. Malkus og M. E. Plesha , Concepts and Application of Finite Element Analysis, New York: John Wiley & Sons, 1989.

[17] T. Haukaas, *Kirchhoff and Mindlin Plates,* Vancouver, 2019.

[18] DNV GL, GeniE Vol.3- Modelling of Plate/shell structures, DNV GL, 2016.

[19] DNV, “FEATURE DESCRIPTION Sesam Software suite for hydrodynamics and structural analysis of renewable, offshore and maritime structures,” DNV, 01 04 2022. [Online]. Available: https://www.dnv.com/Images/Sesam-Feature-Description_tcm8-58834.pdf. [Accessed 03 04 2023].

[20] DNV, DNV- RP_C205, ENVIRONMENTAL CONDITIONS, DNV, 2021.

[21] A. Bakharev, Tresca stress 2D, 2005.

[22] Bbanerje, TimoshenkoBeam, 2012.